Technical Report

AN EXPERIMENTAL STUDY OF WIND FORCES ON OFFSHORE STRUCTURES

by

John H. Nath
Associate Professor of Civil Engineering
Colorado State University

Prepared for

The National Science Foundation
Grant No. G.K. 4679

August 1970

CER70-71JHN3

ABSTRACT

This experimental study verified that the pressure coefficients and the total drag coefficient are reduced for a structure when it is elevated on supports. The jet of air under the structure reduces the magnitudes of both the positive pressures on the upstream face of the building and the negative pressures on the downstream face. In addition, it is indicated that for offshore structures and other elevated ocean structures that the drag coefficient increases drastically on the windward face of a wave.

ACKNOWLEDGMENTS

With gratitude it is acknowledged that the principal financial support for this study was provided by the Engineering Division of the National Science Foundation. In addition, the Chevron Oil Field Research Corporation at La Habra, California augmented the financing so that Mr. Cheong was able to stay with the project for the entire academic year. The experimental portion of the work dealing with wind forces on buoys was supported by the Convair Division of General Dynamics, San Diego, California.

In particular, the very fine assistance of Mr. Hin Fatt Cheong has been gratefully accepted. Never has the author been so fortunate as to have had such an able and intelligent assistant.

TABLE OF CONTENTS

INTRODUCTION

Background Information and Scope

A very large number of offshore structures have been constructed to explore for and extract oil from below the ocean floor. This activity has increased to where the oil thus produced represents a very significant percentage of the total crude oil produced in the world. These structures must be designed to safely withstand the forces from the harsh marine environment in order to protect the lives of the workers on board and to protect the equipment and the environment itself from serious failures.

The wind causes very significant forces on such structures, yet little is known about the true distribution and magnitude of wind pressure forces acting on ocean platforms. For predicting the wind forces on ocean platforms, most designers rely upon information from professional journals and reports which have been developed for land based structures. One widely used report is from the American Society of Civil Engineers Task Committee on Wind Forces entitled "Wind Forces on Structures" (6). However, a preliminary study by the author indicated that the drag coefficients obtained for land based structures may be considerably too large for ocean structures because the structures at sea are usually elevated a considerable distance above the water surface on their supporting legs. The resulting jet of air under the structure in effect reduces the drag coefficients.

In order to predict the drag forces on structures with a good degree of precision one must know the character of the wind field around the structure. One part of this investigation is an initial attempt to define the wind field at sea based on the existing literature and from the viewpoint of the designer. The second part of this investigation is a laboratory wind tunnel study of the drag forces on a few basic structural shapes, such as a cube, a sphere and a simulated platform with and without a drilling tower. The objects were tested in a smooth wind tunnel and in a condition of a rigid sinusoidal wave constructed on the floor of the tunnel.

Review of Pertinent Literature

A very large fund of literature is growing on the subject of wind forces on land structures and on the character of the atmospheric wind field. That which is pertinent to the wind field at sea is covered in the next section and only that which is pertinent to this laboratory study is presented here.

Several texts present the classical drag coefficient vs. Reynolds number relationship for circular cylinders that are essentially infinite in length and for spheres, as shown here in Figure 1. Reference 3 also gives values of drag coefficient for other shapes. The data for circular and square cylinders and for rectangular plates are reproduced here in Table 1. Reference 6 presents drag and lift coefficients and Strouhal numbers for a variety of common shapes of structural members used by the building industry.

The drag coefficient, C_D , is defined in the usual way, such that

$$F_D = C_D \frac{A\rho V^2}{2} \qquad (1)$$

where F_D is the total drag force, A is the projected area, perpendicular to the flow for form drag, which is of interest here, ρ is the mass density of the fluid and V is the ambient velocity, sometimes taken as the rms velocity on the structure and sometimes taken as the velocity at the top of the structure.

Baines (4) performed wind tunnel tests on several model shapes of buildings to investigate the effects of velocity distribution on wind loads and flow patterns. One shape tested was the cube. One can derive from the pressure distributions presented that the total drag coefficient for a cube suspended in the free stream velocity and oriented with one face perpendicular to the flow is 1.25.

As stated in the discussion for the above paper, the scale of turbulence in the wind tunnel tends to be much smaller than the structure whereas the scale of turbulence in the atmosphere is usually much larger than a prototype structure. However, at sea one would expect the scale of turbulence to be at least approximately proportional to the wave sizes, or surface roughness of the water. For this laboratory work it is expected that the turbulence scale was about in the same proportion to the model as the similar condition for prototype structures.

Free stream turbulence can influence the drag coefficient for a structure. Roberson and Rutherford (16) showed that the drag coefficient on a cube in free stream flow was reduced from about 1.5 to about 1.0 or 1.1 for Reynolds numbers greater than 6000 when the turbulence intensity was increased from 0.6% to 10% with screens upstream from the test specimen. Their work indicated that the horizontal macro scale of turbulence had little if any influence on the drag coefficient.

The wind velocity at sea does vary to some degree with respect to the position on the wave. This variation is an acceleration and the added mass effects on the structure should be considered. A similar condition existed for this study. Yu (25) determined experimentally the added masses of rectangular plates and parallel pipeds in water. The added mass, M , of a rectangular parallel piped having dimensions 2a, 2b and 2c moving perpendicularly to the 2a x 2b face was expressed empirically in the C.G.S. units as

$$M = \rho\left[\frac{6.3\ a^2b^2}{(a^2+b^2)^{\frac{1}{2}}} + 3.5\ ab\sqrt{c}\right] \qquad (2)$$

where ρ is the mass density of the water.

Roshko (17), presented evidence that the drag on circular and non-circular cylinders is related to the shedding frequencies of the vortices. Although of significant value to the basic understanding of the drag phenomena for long cylinders, the paper has little application to the complex structures used in this study.

A preliminary experimental study on drag coefficients for offshore structures was conducted by Nath and Aiston and reported on in Ref. 1. They found that the total drag force on a model structure could be most accurately predicted by considering the tower separately from the rest of the structure. Models were tested in thin and thick boundary layer conditions and the proportion of cylindrical support surfaces of the models had considerable influence on the total drag coefficient for the thin boundary layer condition but they were insignificant for the thick boundary layer condition. The angle of wind incidence on the structure had only a slight influence on the drag coefficient. The significant point that was determined was that the total drag coefficient was about equal to or less than 0.9, which is considerably less than that for an equivalent land based structure not supported above the ground on legs. The equivalent coefficient for similar land based structures would be between 1.2 and 1.5 according to Ref. 6. The lower coefficient was attributed to the jet of air under the structure, which reduces the positive pressures to some degree on the upstream face of the structure and reduces the magnitude of the negative pressures considerably on the downstream face.

The magnitude of the wind forces on the various components of ocean platforms depends a great deal on the character of the wind at sea. Present knowledge indicates that the wind field is quite variable, depending on location and the thermal stability of the wind. The next section of this report

represents a preliminary attempt at defining the wind field at sea with the interests of the designer of offshore structures in mind.

THE WIND FIELD ABOVE THE OCEAN

A considerable volume of literature exists on the description of the wind field above the undulating ocean surface. However, a great deal of it is about theoretical or laboratory studies. With respect to the fact that the oceans cover 71% of the surface of the earth only a miniscule amount of information exists on quantitative measurements of the wind field at sea.

Because this review is primarily concerned with wind forces on offshore structures, little attention will be given to altitudes above 1000 feet or to offshore winds, which are less intense than ocean or onshore winds. Since design information is desired, only the strong winds that blow for a considerable period of time from one horizontal direction, or azimuth, will be considered. However, the two-dimensional turbulent aspect of the air flow will be considered. It is true that vortex shedding and three-dimensional turbulence can induce significant forces on structures but they are due to the interaction between the flow and the structure and are not considered to be within the scope of this section.

The sequence of presentation will be the shape of the velocity profile, the wind magnitude, the magnitude and

structure of gusts, then the coupled influence from the waves and how they influence the velocity and pressure structure directly above them.

The Shape of the Velocity Profile

The measurements that exist on the shape of the velocity profile of the wind above the ocean vary considerably. Generally, it seems that the logarithmic profile occurs more frequently than others. The variability is not surprising when one considers the thermodynamic activities as well as the dynamics. A crude example would be the conditions where the water is warm and the air is cold. Then thermal energy will flow from the water to the air where some of it is transformed into kinetic energy. This added kinetic energy can feed back into the water waves but the point here is that one would not necessarily expect the same velocity profiles to exist when the kinetic energies are being modified by the transfer of thermal and kinetic energy, either from the water to the air or the air to the water. Furthermore, during transient conditions of energy transfer the synoptic wind velocity profiles may have different general shapes with respect to horizontal location.

Miles (11) has published several articles on the generation of surface waves by shear flows wherein the logarithmic profile is assumed. Kinsman (10), however, feels it is impossible to sustain a logarithmic profile because of energy exchange from the wind to the water.

Even though there are uncertainties, the engineer of today must make some assumptions as to the velocity profile if it is necessary for him to design for the realistic situation. The largest part of recent contributions to the literature indicate that the velocity profile, near but not at the water surface, is logarithmic, taking the form:

$$\frac{u(z)}{u_*} = \frac{1}{K} \ln \frac{z}{z_o} \tag{3}$$

wherein $u(z)$ is the wind velocity, z is taken as positive upward as shown in Figure 2, u_* is the friction velocity, K is the von Karman constant, generally taken equal to 0.4 and z_o is the aerodynamic roughness. The friction velocity is expressed as,

$$u_* = \left(\frac{\tau_o}{\rho} \right)^{\frac{1}{2}} \tag{4}$$

wherein τ_o is the mean surface shear stress and ρ is the mass density of the air. If Eq. 3 expressed the measured velocity profiles precisely, then one could calculate τ_o and z_o from the two simultaneous equations that arise from considering conditions at two values of z. Then τ_o and z_o would remain constant regardless of the two values of z used. However, it is found that there are variations of the mean profile from the logarithmic, so that some sort of averaging procedure must be used for determining τ_o and z_o.

The value of the aerodynamic roughness, z_o, depends on the aerodynamic roughness of the sea surface, which in turn depends on the magnitude and duration of the wind and length of the fetch. The aerodynamic roughness for wind blowing over land, trees, crops or relatively smooth surfaces is supposedly only a function of the absolute roughness of the surface. In the laboratory, or for any small scale flows, the roughness can be expressed in terms of an equivalent sand grain roughness. The surface shear stress is then expressed in terms of a dimensionless drag coefficient,

$$\tau_o = C_f \frac{\rho u_a^2}{2} \tag{5}$$

wherein u_a is the ambient or gradient velocity and C_f is the local drag coefficient. It is known that the drag coefficient is a function of the aerodynamic or equivalent sand grain roughness and the Reynolds number:

$$R_e = \frac{u_a L}{\nu} \tag{6}$$

wherein L is the distance from the equivalent leading edge of the surface and ν is the kinematic viscosity of the fluid. Plots of C_f vs. the Reynolds number exist in many texts, notably in Schlichting (19).

A different situation exists for water waves. As the Reynolds number increases, say, by increasing the fetch, assuming the sea is not time limited, the aerodynamic roughness will increase asymptotically up to the saturation limit

where the net exchange of energy from the wind to the sea becomes zero. Some information exists for the values of the aerodynamic roughness, z_o , at sea, however it is not plentiful and indicates that much work needs to be done on this topic.

Monin (12) shows that z_o depends on the local wind velocity and that for strong winds the sea-surface resistance to wind flow changes with fetch and time. For fully developed waves (which is likely to be a design condition for offshore structures) the average wave height exceeds 100 h_s , where $h_s >> \nu\, u_*$ and ν is the kinematic viscosity of the air. For such conditions, z_o may be estimated from

$$z_o = 0.035 \frac{u_*^2}{g} \quad . \tag{7}$$

Equation 7 was obtained from experimental data.

Generally, drag coefficients are considered to be functions of Reynolds number and surface roughness, or object shape. However when a surface is hydrodynamically rough the drag coefficient is independent of Reynolds number. Wu (24) attempted to correlate the drag coefficient for a hydrodynamically rough water surface based on the Froude number. He argued that principally form drag is present and that for a completely rough surface the drag coefficient is independent of the Reynolds number. His relationship for the drag coefficient was:

$$\frac{1}{C_f^{\frac{1}{2}}} = \frac{1}{K} \ln \left(\frac{1}{aC_f F^2} \right) \tag{8}$$

wherein a is a constant developed by Charnock (5) characterizing the equilibrium condition between the wind and the disturbed water surface with a value of 0.0112 and F is the Froude number defined as follows:

$$F = \frac{u}{(gz)^{\frac{1}{2}}} \quad . \tag{9}$$

Using data from twelve laboratory studies and thirty oceanic observations, Wu justified Eq. 8. However, if one plots the basic data presented by Wu on log-log paper he finds that the data is scattered about a straight line with little more scatter than that which is shown by Wu about Eq. 8. Therefore, using empirical techniques one can develop the simple expression,

$$C_f = 0.0017\ F^{\frac{1}{2}} \quad . \tag{10}$$

Now, given the wind velocity at some height, say at $z = 10$ m, C_f can be calculated from Eq. 10 and the aerodynamic roughness can be calculated from Eqs. 3, 4 and 5. According to the values shown, Wu's study includes data from oceanic winds of from about 15 kt to 60 kt.

In an extensive survey, Ruggles (18), showed that more than 90% of the profiles were logarithmic from a set of 299 mean wind profiles. Wind speeds ranged from 2 kt to about 20 kt. The seas were composed of deep water waves and were not fetch limited. With considerable scatter involved, it was shown that shear velocity was linearly related to the 10 meter wind speed as,

$$u_* = 0.04\ u_{10} \quad . \tag{11}$$

Ruggles also plotted the aerodynamic roughness, Z_o versus the 10 m wind speed and the results showed peaks due to such effects as the transition from capillary waves to longer waves, etc., and are probably not of engineering significance. A value of z_o that is fairly constant in his data seems to be between 0.1 and 1.0 cm. It is unfortunate that Ruggles did not explain how the shear velocity and aerodynamic roughness was deduced from the field measurements.

Davenport (7) suggested that a simple power law can be used for the velocity distribution, namely,

$$u(z) = u_a \left(\frac{z}{z_a}\right)^{1/\alpha} \tag{12}$$

wherein u_a is the gradient, or free stream velocity which exists at the boundary layer thickness, z_a . The suggested value of α for winds over water was 8.5 and the value of z_a was 244 m. Given the design wind velocity at 10 m, the gradient velocity can be calculated, and then the entire profile determined.

Thermal stratification of the air causes considerable deviation in the velocity profile. Much work has been done on this subject but it is inconclusive thus far as to how this phenomenon effects the design of offshore structures. This topic deserves additional study.

Due to the Coriolis effect, the wind velocity is not a two-dimensional curve. The Ekman spiral concept shows that the wind velocity direction at large elevations is considerably different than at the sea surface. However, the deviation within the height of offshore platforms will probably be small enough so that the velocity profile can be considered to be two-dimensional for design purposes.

As the reader can surmise, a great deal of uncertainty still exists as to the true shape of the wind velocity profile at sea. Measurements display a great deal of scatter, and they should because many variables influence the velocity profile. It makes a great deal of difference whether the wind is increasing in intensity or decreasing or remaining constant (an unlikely occurrence) or if the fetch is such that the profile is influenced from adjacent land masses. Thermodynamic influences due to different temperatures between the air and water also influence the shape of the velocity profile. Thus the designer who needs to know the shape of the velocity profile is justified in using either Eq. 3 or Eq. 12 until an adequate quantity of data and information becomes available that clearly shows one specific relationship to be the best choice.

The Magnitude of the Mean Wind

Thom (23) has collected many records of extreme winds in the United States and reduced them by means of the 1/7th power law to the wind at an altitude of 30 ft, or 9.15 m. He

determined that he had enough data to be able to predict winds with a confidence interval of 0.90. The extreme mile wind speed was recorded (the one-mile passage of wind with the highest speed for a day). Although he did not report on winds at sea, he did include coastal areas. The winds were related to the mean recurrence interval, as calculated from

$$R = 1/[1 - F^2(x)] \tag{13}$$

wherein R is the mean recurrence interval and F is defined as:

$$F(x) = P[s < x] \tag{14}$$

or

$$F(x) = \exp - \left(\frac{x}{B}\right)^{-\gamma} \tag{15}$$

wherein $P[\ ]$ reads "the probability that", s is the wind speed, x is the limiting wind and γ and B are determined from the method of maximum likelihood. His results for coastal areas were:

(all velocities in kts.)

MEAN RECURRENCE INTERVAL (yrs)	PACIFIC COAST		GULF	ATLANTIC	
	Cal.	Ore.		Below Maine	Maine
2	26	52	44	48	48
50	58	83	87	104	87
100	70	87	96	113	96

In 1969 Hurricane Camille had winds in excess of 150 kts in the Gulf of Mexico and produced many millions of dollars of

damage to offshore structures. Certainly the designer should be conservative in most cases in selecting a design wind velocity.

The design wind will depend on the geographical location of the structure as noted above. Lacking other information, a wind velocity of 150 kts is frequently used.

Wind Gusts

Wind turbulence, or gustiness, can have various effects on an ocean structure. The most obvious effect is the temporary increase in wind velocity to which a structure is subjected and the second action is the repetitive mode of application of this increased load. The eddies, or vortices, that exist can vary in size, and, since they are carried along with the somewhat constant mean wind, they occur over some frequency band. It may be possible for a component frequency to be equal to a modal frequency of the structure and induce a resonant condition that can be quite harmful if the fluctuating load persists.

Davenport (8) attempted to give design information about gusts that include not only the increase in pressure on a building but the effects from resonance as well. Unfortunately the equations are quite cumbersome and based on empiricisms. One feels that if an empirical approach is taken, it should be simple, particularly in view of the uncertainties injected by mother nature. He defined the temperal maximum pressure as:

$$p(z)_{max} = G\ \bar{p}(z) \tag{16}$$

where $\bar{p}$ is the mean wind pressure at the point x on the structure and G is the gust factor defined as:

$$G = 1 + gr\sqrt{B + R} \tag{17}$$

wherein g is a peak factor, r is a roughness factor and would appear to have a value of from 0.1 to 0.25 for water, B is structural excitation by background turbulence with a suggested value of around 1.5 and R is the excitation by turbulence resonance with the structure. In the above expression, R is given by:

$$R = \frac{SF}{\beta} \tag{18}$$

where S is a size reduction factor, F is a gust energy ratio and β is a damping factor. The peak factor, g, is a function of the natural frequency of vibrations of the structure and the total time of load application and can vary from 2.5 to 4.5. The value of F depends on the wave number and resonance number and by this time one is ready to forget the whole thing because the contact with reality has been completely lost. However, by persisting through the article one finds that the value of G can be about 1.5, which says that the gust velocities fluctuate above and below the mean value by about 50% of the mean value.

Sherlock (22) suggested that it is adequate to assume the 1/7 power law for the velocity distribution up to a

height of 1000 feet and that the corresponding gust factor would be 1.5 for a height of 30 feet and 1.15 at about 2000 feet.

The frequencies of the turbulent gusts depend on the boundary conditions as well as certain internal fluid dynamic and thermodynamic instabilities. One may surmise that the water wave spectrum would influence the turbulent frequencies to some degree and this is born out in the reference by Seesholtz and Mollo-Christensen (20). Figure 3 is taken directly from that reference, which shows that within the range measured the turbulence frequencies have two distinct ranges, one that is equivalent to the wave frequencies and the other, containing greater energies, at about 0.03 to 0.04 Hz, which are presumably due to internal conditions.

For structures that are built in deep water a resonance problem may exist if the frequency of the waves corresponds to any of the first few modes of vibration of the structure, depending on the geometry of the supports. Such problems are considered in Nath and Harleman (13). Figure 3 indicates that wind gust frequencies can coincide with wave frequencies so that a doubly dangerous condition could arise if resonance to waves exists.

The wind flow pattern above the sea is particularly of interest to this study. Testing was done in a wind tunnel with a solid wave built into the floor and the question should be explored as to whether the flow pattern resembled that at sea even approximately.

Shemdin (21) reviewed the several basic theories of wave generation by wind and showed the importance of the region below the critical layer and above the water surface. The critical layer is defined such that the upper extremity is where the wind velocity is equal to the phase velocity of the wave.

Measurements of velocity profiles and pressure distributions showed that there was only little, if any, separation of the wind flow pattern downstream of a wave crest. However, such measurements have never been made for very high and steep storm waves at sea. Accepting the information that is available - it appears that the logarithmic velocity profile may be raised and lowered in its entirety as the wind flows over a wave crest and trough, respectively. However, it should be remembered that many investigators believe that the logarithmic velocity profile can only be valid at several roughness heights above the boundary. Thus, according to Shemdin, the wind velocity at a fixed small distance above the mean water surface is higher over the trough than over the wave crest. This was indicated by Seesholtz and Mollo-Christensen where cross-correlation between wind velocities and water surface showed maximum wind velocities just slightly downstream (about 60 degrees phase shift) from the wave trough.

The ambient pressure distribution was measured by Seesholtz and Mollo-Christensen at sea and by Shemdin and Hsi in the laboratory. The former investigators had a fixed

transducer at about 1.2 meters above mean sea level in the vicinity of the critical layer and found that the maximum pressure occurred just above the wave trough. The later investigation showed that the maximum pressure occurred over the crest of the wave for low wind velocities and gradually shifted to a position generally over the trough as the wind velocity was increased when the pressure probe moved with the water surface, staying within the critical layer. Shemdin and Hsi also showed that for a probe fixed above the wave crests, that the pressure was greatest over the trough for all velocities. The magnitudes of the pressure variations were not indicated but must have been fairly small so that this facet of the problem may not be of great interest to the designers of ocean structures. However, this point should be explored more fully.

It has been shown how the designer of an ocean structure can estimate the wind field above the ocean as a first step in determining the wind forces acting on the structure. The average magnitude of the wind can be estimated using some assumed mean recurrence interval and the vertical velocity distribution can be calculated from the logarithmic profile equation. The magnitude of wind gusts can be estimated and it can be assumed from the above information that the maximum velocities occur about over the wave troughs.

It should be emphasized, however, that the above information is based on sparse data and that any final design

should include a fairly large factor of safety that is established in accordance with the use of the structure.

The laboratory work for this study will show how the wind drag coefficients vary for different types of offshore structure.

LABORATORY EXPERIMENTATION

Description of the Equipment

Practically all of the testing for this study was performed in the relatively low speed Colorado State University Wind Tunnel which is located in the Fluid Dynamics and Diffusion Laboratory at the Engineering Research Center. This wind tunnel, which is presented in Figure 4, has a test section of 30 feet length and a nominal cross-sectional area of 6 feet by 6 feet. The wind tunnel drive is provided by a 75 hp 16 blade axial fan with the speed controlled by a pitch control motor. Test section air velocities range from about 5 to 60 ft/sec.

The recent work was accomplished with a smooth flat floor, or a thin boundary layer condition, and with a smooth sinusoidal wave built on to the floor. Earlier work by Nath and Aiston utilized both a thin boundary layer condition (where the boundary layer was less than or equal to 2 inches thick) and a thick boundary layer (where the boundary layer was about 14 inches thick) which was developed by stapling a dense mat of small plastic tree limbs to a false floor on the tunnel for the full 30 feet of the test section.

The smooth wavy surface consisted of a ¼ in. thick plywood shell screwed in place to 4 parallel rows of wooden stiffeners that conform to a sinusoidal curve with an amplitude of 2.6 in. and a wavelength of 6 feet. The C.S.U. wind tunnel could accommodate 5 complete waveforms. Figure 5 shows a longitudinal section of the waves. At a 1:100 scale, this wave represents a prototype wave 600 feet long and 43.3 feet high. In deep water this represents a wave with a period of eleven seconds, which represents the component with considerable energy in many measured wave spectra.

A small amount of this work was accomplished in the Meteorological Wind Tunnel in the same Laboratory. This tunnel was constructed by Colorado State University for the U.S. Army under Contract DA-36-039-SC-80371. The tunnel features a test section of 88 feet length and a nominal cross-sectional area of 6 ft by 6 ft with a movable ceiling which can be adjusted for establishing negative and positive longitudinal pressure gradients or a zero pressure gradient. A large contraction ratio at the entrance of 9 to 1 in conjunction with a set of four damping screens yields an ambient turbulence level of about 0.1 percent. Test-section air velocities range from about 0 to 125 ft/sec.

For direct measurements of drag forces, a shear plate was used. The term "shear plate" evolved for this instrument because it was originally developed by Nath to measure the shear stress at the wall in boundary layer flow. The shear plate was made of aluminum plate which had the dimensions

24 in. x 24 in. x 3/4 in. This plate was separated from the foundation plate by three chrome-steel balls. The ball diameter was 1/4 in. Two stainless steel restoring arms, 1/8 in. x 1/2 in. x 18 in. each, were used. One end of the arm was thoroughly fixed to the shear plate and the other end was equally fixed to the foundation plate so that no rotation could occur at the attachment points. Four semi-conductor strain gages, one to each side of the restoring arm, were installed at 1/2 in. from the end of the restoring arm which was attached to the foundation plate. The semi-conductor strain gages used for this shear plate were made by Electro-Optical System, Inc., Model No. P01-05-500, type P, which has a resistance of 500 ohms.

For frictionless purposes, the balls were set on hardened, highly polished tungsten cobalt disks which were imbedded in the shear plate and the foundation plate. The shear plate was able to move back and forth horizontally only, and it had a natural frequency 6 cycles per second. A photograph of the shear plate is presented in Figure 6 and a schematic diagram in Figure 7.

The bridge circuitry arrangement of the four matched semi-conductor strain gages on the deflecting beams are shown in Figure 8. The shear plate is a linear device capable of measuring drag forces from 0.00022 to 7 pounds. It is limited on the low range by the stability and sensitivity of the electronic equipment and on the high range by the elastic strength of the restoring arms. It was experimentally proven

that the shear plate will return to its original position after the applied force is removed. Power for the shear plate is supplied by an 8-volt D-C supply and the output voltage readout device is a D-C mili-micro-voltmeter.

For calibration purposes, a vertical support can be screwed on to the movable plate. The shear plate is calibrated by suspending known weights on a string which passes over an almost frictionless pulley and is attached to the vertical support. The plate was calibrated with a model on it. A typical calibration curve is presented in Figure 9.

The wind velocity profile was measured with a Prandtl tube which was mounted on a carriage with transverse and vertical movement mechanism. The position of the Prandtl tube was sensed by an attached potentiometer. The difference between static and dynamic pressure of the flow was read from a Trans-sonic Type 120 B Equibar pressure meter. This pressure meter operates over a total pressure range of 0-30 mm Hg in eight full-scale range. The readings, in mm of mercury, were converted to velocity in feet per second corresponding to the temperature registered by a thermometer in the tunnel. For vertical or horizontal velocity profiles, the position of the Prandtl tube and the velocity signal from the equibar pressure were recorded simultaneously on an X-Y plotter.

Description of the Model Structures

Four basic structural shapes were investigated for this study--a cube, a sphere, a platform and a platform with a tower attached.

The plain cube measured 12 in. on each edge and was made of plexiglass sheets. Two adjacent faces, a top face and a vertical face, were provided with piezometer taps for the determination of the pressure distribution around the cube. The arrangement of the piezometer taps for each face consisted of three rows with three taps in each row. The spacing between adjacent taps was 4 1/2 ins. The bottom face was a 12 ins. square plexiglass sheet with a circular central hole for leading out the piezometric connections through the wind tunnel floor. The plain cube could be provided with four legs of 1 1/2 ins. diameter plexiglass tubing by removing the original bottom piece and screwing in place another 12 in. square plexiglass piece to which was glued 4 legs 8 ins. in height with 7 in. spacing between adjacent legs.

The platform and sphere models were constructed of styrofoam. For each model, 1 in. diameter wooden dowels were glued into the syrofoam to form the piers supporting the superstructure.

The tower was built with 3/16 in. wooden dowels with each panel braced only on alternate diagonals for simplicity in the construction. Details of the models are shown in Figures 10 through 14.

In addition to the structural models, some drag force determinations were made for two oceanographic buoys. One was a model of an aid-to-navigation buoy, utilized by the U. S. Coast Guard and here abbreviated as the CGB and the other was a model of the Office of Naval Research Ocean Data Station, here abbreviated as the ODS. The scale models (with a ratio of 1:24) were provided by the Convair Division of General Dynamics.

The prototype CGB consisted of a basic disc hull of 40 feet diamater with a central mast of 3 feet diameter for about 16 feet of height. On top of the solid mast was a truss-work of two-inch diameter pipes extending to about 35 feet of height above the deck. On top of the mast was a whip antenna with an average diameter of about 4 inches and a length of about 35 feet.

The ODS was also a basic 40 feet diameter hull but the superstructure was considerably different. The mast varied from a diameter of about 3 feet at the base to 15 inches at a height of 21 inches and a diameter of 10 inches at a height of about 40 feet above the deck. To the mast at this height were attached 24 wires of 5/8 inch diameter that were evenly spaced and attached to the gunwale of the buoy at the lower ends. At the top of the wires were arrayed 20 rods of 14 feet in length arranged like spokes. Above the rods were miscellaneous small items. The wires and rods are referred to as the discone antenna. Photographs of the

two models in the Meteorological Wind Tunnel are shown in Figures 15 and 16.

Procedure

The first part of the experimental work involved testing with a smooth flat floor under the models. The shear plate and particle boards, forming a false floor into which the shear plate was recessed so that the top of the plate was flush with the floor, were positioned and vertical velocity profiles at the position of the shear plate were obtained. Each structure was then taped to the shear plate and drag measurements were recorded for different ambient wind velocities. For the plain cube and platform structure, drag force determinations were made for 3 different angles of incidence of the wind. In addition, the pressure distributions on the plain cube and the elevated cube structure were taken for an angle of incidence of zero degrees. The purpose of this part of the work was to compare the experimental results with those of accepted published information.

After installation of the wave into the tunnel, vertical velocity profiles at different points along the length of the surface were taken. The longitudinal pressure gradient was also determined with the static taps of two Prandtl tubes. Both Prandtl tubes were initially set side by side at the same elevation in the freestream. The pressure difference between both tubes was essentially

zero for any flow velocity. One of the Prandtl tubes was used for reference static pressure, and the other was traversed downstream. The longitudinal pressure gradient of the solid wave condition was thus obtained.

Except for the buoy models, drag force measurements were taken for each structure at the trough, the crest and the 1/4 wave points of the 4th wave at different ambient velocities. The velocity profiles just downstream of the structures for most conditions were also obtained.

For drag force measurements with the structure on the wave, the shear plate was placed on the center-line of the tunnel floor in the lane formed by the two inner wooden stiffeners at the fourth wave. The structures were taped to the surface of the shear plate and projected above the wavy surface. In place of the plywood that had to be removed to allow for the projection, thin metal sheets which were flexible enough to conform to the sinusoidal curve and yet strong enough not to suffer any deformation due to an impressed wind force were taped in place to cover up existing gaps. However, sufficient clearance between the sheets and the legs was allowed for the longitudinal movement of the legs.

EXPERIMENTAL RESULTS

Velocity Profiles

Velocity profiles were taken in the smooth wind tunnels. Figure 17 shows profiles for the C.S.U. wind

tunnel at two different reference velocities. The reference velocity refers to the freestream velocity measured near the upstream end of the test section with a fixed Prandtl tube. Figure 18 shows two velocity profiles taken at the position of the center of the buoy model, without the buoy present, but with a gravel covered ramp that lead to the upstream edge of the buoy. Figure 19 shows velocity profiles taken above the smooth false floor in the Meteorological Wind Tunnel. Figure 20 shows a series of velocity profiles taken by Aiston for flow around a small platform and tower. The platform measured 5 inches square in plan view, or 1/4 the size of the platform in this study. Figures 21 through 26 show velocity profiles which partially illustrate the wakes downstream of the models in the wind tunnel with the smooth floor. The true magnitudes of negative velocities were not determined. Where they were detected with negative readings from the Prandtl tube they are indicated on the figures with slight negative values.

Figure 27 shows a profile of the wave in the tunnel and a series of velocity curves at the troughs and crests for an upstream reference velocity of 50 fps. The boundary layer development is indicated. The boundary layer for reference velocities of about 38 fps and 20.1 fps are also indicated on Figure 27. This figure indicates that the boundary layer did not undulate perfectly with the wave in the wind

tunnel. Instead, along with partially following the wave surface, the boundary layer thickness increases steadily along the length of the tunnel and also changes shape in the lower regions fairly radically from crest to trough to crest. It can also be seen that the boundary layer thickness is rather small in the wind tunnel, being thinner than the height of the structural models in most cases. Thus the ratio of boundary layer thickness to structural height was not modeled from a prototype situation for this work. However, it is felt that the results will be on the conservative side.

Some velocity profiles on the fourth wave, where the models were fairly intensively tested, are shown in Figure 28, plotted on log-log paper. The velocities within the boundary layer are fairly logarithmic, as can be seen and the boundary layer thickness on the fourth wave is shown to be quite constant from the wave surface. Figure 29 portrays typical curves downstream of the crest which show that separation did not occur on the wave in the wind tunnel. Thus, in comparison with the information from some of the references previously cited, the velocity distributions used in this testing more closely approximate free stream velocities that change in magnitude with respect to position on the wave, with higher velocities at the crest than at the trough. According to the citations the velocities at sea are greater above the trough than above

the crest because it is believed that the velocity distribution curve moves along with the wave, being raised at the crests and lowered at the troughs.

Some velocity profiles were taken behind the structures at the various positions on the fourth wave. They are summarized in Figures 30 to 44.

Ambient Pressure

The longitudinal pressure distribution in the wind tunnel was measured and is presented in Figure 45. The figure shows that the mean pressure decreases because of the head losses in the wind tunnel and that the pressure fluctuates in the wind tunnel in accordance with the changing cross-section and Bernoulli's equation. Reference 20 indicates that the ambient pressure at sea may be about 180^{o} out of phase with the surface waves. This would indicate that perhaps the pressure distribution in the wind tunnel is at least analogous to the sea condition. However, the pressure variation at sea is probably much smaller than that experienced in this study. It should be pointed out that as previously stated, Ref. 21 shows that the phase shift between ambient pressure and the wave surface depends to some degree on whether the pressure transducer follows the water surface and thus remains inside the critical layer (the pressure was about in phase with the wave) or whether the transducer was at a fixed position outside the critical layer (the pressure was about out of

phase with the wave). Most offshore structures are constructed above the critical layer, so that the pressure distribution obtained in this study should at least approximate the trend in the pressure fluctuations at sea.

It can be concluded from the above information that the environment generated in the wind tunnel for this study did only roughly approximate that at sea. The major differences were that the boundary layer was much thinner in the wind tunnel, being only a fraction of the height of the structure instead of being considerably longer than the structure height; the ocean structures are submitted to spray, which should create a sizeable wind driven force that is not modeled in the wind tunnel; the Reynolds number in the model was considerably less than that which is experienced at sea but this was accounted for as explained later. The major similarities between the laboratory study and sea conditions are that the velocity distribution within the boundary layer was approximately logarithmic and the phase relationship between the ambient pressure and the wave surface was about equal to that at sea, according to some published information.

Drag Force Determinations

Wind tunnel with smooth floor - Several drag force determinations were made on the various structures with the wind tunnel with the smooth floor. The purpose was to compare results with known results in the literature for similar work.

The plain cube was tested by determining the pressure distribution on it and by testing it on the shear plate. The pressure coefficients are given in Figure 46 for two different wind velocities, or Reynolds number, and for an angle of incidence of zero degrees. The total drag coefficient was computed by integrating the pressure coefficient volumes over the front and the fear faces of the plain cube. A similar operation was performed on the data presented in Ref. 4. Figure 47 presents the drag coefficient summary for the cube with various angles of incidence where the drag forces were measured with the shear plate. A comparison of the drag coefficients for zero incidence and for high Reynolds number is given in Table 2. The table shows that the result of the shear plate measurement agrees well with Ref. 4, and is about 6% different from the result obtained by measuring the pressure distribution on the cube.

The elevated cube was tested at zero incidence only. The pressure coefficients are shown in Fig. 48 for two values of the Reynolds number. In comparison with Figure 46 it can be seen that there is a definite reduction in the pressure coefficients when the cube is elevated on its supports. The drag coefficients for the cube alone were calculated by integrating the pressure coefficients on the upstream and downstream faces. They were also determined

from the shear plate measurements by deducting the effect on total drag due to the cylindrical supports. That is, by referring to the velocity profiles taken without the structure present the rms velocity acting on the legs can be determined. The Reynolds number is low so that the drag coefficient is 1.2. The comparison of drag coefficients is made in Table 3. It can be seen that there is fairly good agreement between the values. The drag coefficients for the elevated cube are about 32% smaller than those for the plain cube resting flat on the wind tunnel floor at comparable Reynolds number. The results in Table 3 also indicate that some shielding of the downstream supports from the upstream ones does exist. A drag coefficient of 1.2 was used for the legs and the projected area of all four legs. Thus the coefficients measured with the shear plate appear a little smaller than those measured with pressure distribution.

The sphere structure was tested in the smooth floor condition with the shear plate at a Reynolds number of 3.4×10^5--very close to the critical Reynolds number as shown in Figure 1. The total drag coefficient was 0.52 whereas that for the sphere alone (after deducting the effects of the supports) was 0.40. For sub-critical Reynolds number it is about 0.50, depending on the Reynolds number, as indicated in Figure 1. A photograph of the sphere structure on the shear plate in the smooth wind tunnel is presented as Figure 49.

The platform with the large rough legs was tested at several Reynolds numbers and angles of incidence. The total drag coefficients were calculated from Eq. 1 using the total projected area, including the legs, and the rms wind velocity, with respect to height, acting on the structure. The results are shown in Figure 50. Aiston (2) determined that the total drag coefficient for zero incidence should be about 0.62, so that the agreement is close.

The platform with tower with the large rough legs was tested similarly to the above test. The results are presented in Figure 51. Aiston obtained a total drag coefficient of about 0.60, which agrees within 14% of the results from Figure 51 for zero incidence.

Aiston tested with a thin boundary layer and a thick boundary layer with several conditions for the structures. A summary of the results of the average drag coefficients are presented in Table 4.

The buoys were tested at various wind velocities in the smooth wind tunnel condition only in both the C.S.U. tunnel and the Meteorological Wind Tunnel. A theoretical drag force was determined for each condition by calculating the Reynolds number and thence the drag coefficient for each element of the buoy. If the length-to-diameter ratio of a cylindrical unit of the model was greater than 20, then the drag coefficient was selected from Figure 1. For other values

of the ratio, the drag coefficient was selected from Table 1. The total calculated drag force was then compared with the measured drag force. Close agreement occurred for all experimental conditions, indicating that it is reasonable to proceed in such a manner for prototype calculations.

The models were taped to the shear plate and placed at the upstream end of the wind tunnel test sections so that they would be subjected to a nearly uniform velocity profile. The boundary layer thickness for the C.S.U. wind tunnel was very small whereas for the long wind tunnel it was appreciable. It was desired to have a velocity profile with a steep gradient over the height of the models and this condition was easily obtained in the long tunnel, at the upstream end.

In the C.S.U. Wind Tunnel only the CGB was tested - both with and without simulated cone antenna wires. The buoy was merely placed downstream of a ramp-shaped transition section that roughly simulated the degree of submergence of the prototype buoy in the water.

A false floor, 2 1/2 inches thick, was installed in the Meterological Wind Tunnel so that the models were "submerged" exactly 1 3/4 inches, which simulates the prototype condition in still water. Figures 15 and 16 show the arrangement of the false floor and model set-up in the Meteorological Wind Tunnel.

The drag forces on the models were calculated by considering the various portions of the models individually.

of the ratio, the drag coefficient was selected from Table 1. The total calculated drag force was then compared with the measured drag force. Close agreement occurred for all experimental conditions, indicating that it is reasonable to proceed in such a manner for prototype calculations.

The models were taped to the shear plate and placed at the upstream end of the wind tunnel test sections so that they would be subjected to a nearly uniform velocity profile. The boundary layer thickness for the C.S.U. wind tunnel was very small whereas for the long wind tunnel it was appreciable. It was desired to have a velocity profile with a steep gradient over the height of the models and this condition was easily obtained in the long tunnel, at the upstream end.

In the C.S.U. Wind Tunnel only the CGB was tested - both with and without simulated cone antenna wires. The buoy was merely placed downstream of a ramp-shaped transition section that roughly simulated the degree of submergence of the prototype buoy in the water.

A false floor, 2 1/2 inches thick, was installed in the Meterological Wind Tunnel so that the models were "submerged" exactly 1 3/4 inches, which simulates the prototype condition in still water. Figures 15 and 16 show the arrangement of the false floor and model set-up in the Meteorological Wind Tunnel.

The drag forces on the models were calculated by considering the various portions of the models individually.

That is, the hull was considered as one unit and so were the mast, antenna wires and the truss work. The Reynolds number for each unit was determined by using the characteristic length of each unit, i.e., the diameters of the cylindrical parts and the diameter of the hull, and the rms wind velocity to which each unit was subjected. The drag coefficients were determined from Figure 1 and Table 1. The total computed drag forces were then compared with the measured drag forces. The results of the computations are presented in Tables 5, 6, and 7.

For the calculations it was assumed that there was no shielding of any cone wires. That is, the projected area of the cone wires was assumed to be equal to the diameter of a wire times the length times the number of wires. Considerable shielding does exist for some of the disc rods at the top of the mast for the ODS and it was assumed that the equivalent projected area was equal to 70 percent of the sum of the projected area of each rod. For the truss work at the top of the CGB the projected area was assumed to be equal to twice the area of the bars on one side of the truss work.

Figure 52 shows some results of Table 7 plotted on a log-log scale. For the higher velocities the measured drag force was exactly proportional to the square of the velocity. The Figure shows that the forces on the CGB model were smaller in the Meteorological Wind Tunnel because

of the improved false floor arrangement. The difference in the drag force for the model with the cone wires and the force on the model without the cone wires gives the amount of the force on the cone wires. The actual equivalent projected area of the cone wires was then calculated from the experimental forces and the drag coefficient as illustrated in Table 6. It was found that the equivalent area was 60% of that shown in Table 6. Because the mast of the ODS is smaller than the mast of the CGB it is expected that there should be less shielding of the wires for the ODS. Therefore an assumption that 80% of the total projected area of the cone wires was used to correct the computed drag forces in Table 7 for the ODS. The resulting average percent difference was +1.3 whereas the average percent difference in Table 7 is +8.3. This would appear to be a trivial difference except for the fact that a disproportionately high drag force exists on the cone wires for the prototype because the Reynolds number is below the critical value for the wires. That is, low drag coefficients should be used for the mast and hull because of their high Reynolds numbers and high drag coefficients on the wires and top assembly because of their low Reynolds number, for the prototype.

Wind tunnel with wave - The structural models were tested on the fourth wave in the C.S.U. wind tunnel. Each model was positioned at 1/4 wave length downstream of the fourth crest, at the fourth crest, at the 1/4 point

upstream of the fourth crest and of the trough between the fourth crest and the third crest. These positions and the four different models are illustrated in Figures 53 through 56. In addition, longitudinal views of two typical installations are shown in Figures 57 and 58. Several wind velocities were imposed on each structure.

The resulting data is presented in two ways. The first presentation includes a comparison of the "theoretical" drag forces vs. the measured drag forces. The quotation marks refer to the fact that known drag coefficients are used for each component part of the structure. The coefficients, in turn, were all originally determined experimentally, of course. The following considerations were made in computing the drag forces. The rms velocity (with respect to elevation) was used as the characteristic velocity on each element of the structure. The Reynolds number was then determined for each element and the drag coefficient was determined from Figure 1, Table 1, or, in a few cases, from the results of the testing in the smooth wind tunnel. The effects of the longitudinal pressure gradient on the superstructures were taken into account and the added mass effect which arises from the convective acceleration that exists as the ambient velocity changes in accordance with the changing section of the wind tunnel. The effects from blockage were included, but found to influence the results by less than 9% at the most.

The procedure was to select a representative velocity profile, taken without the structure present, which had a reference velocity close to that taken at a time of measurement. The profiles used are presented as Figure 59. It was assumed that the acting velocity profile was similar in shape so that the rms velocity acting on any portion of the structure could be determined. The total force acting on the structure was then due to drag forces on the legs, superstructure and tower, the pressure gradient in the tunnel, the added mass effect due to fluid acceleration and blockage. The results are displayed in Tables 8 through 11. It can be seen that the agreement between computed drag and measured drag was fairly good except for the sphere structure and for the platform with and without the tower at the 1/4 wavelength upstream of the fourth crest. The poor results for the sphere structure are understandable since, unfortunately, the Reynolds number turned out to be at the critical values and selecting the correct coefficient for the sphere, a priori, is not possible. For example, the results would be quite good if the drag coefficient for the superstructure had been selected as 0.3 instead of 0.2. This was done for the case at the 1/4 point upstream of the crest where a coefficient of 0.5 was used. It has not yet been determined why the results for all the structures

except the cube are considerably poor at the 1/4 point upstream of the crest. This has been left for future investigation.

The second method of data presentation was to compute, for each structure and position, the total drag coefficient, which was based on the rms velocity of the entire structure, the frontal area of the superstructure, the projected area of all four supports, and twice the frontal area of the tower. The experimental drag forces were first plotted on log-log paper against the rms velocities. The results are presented here as Figures 60 through 63. For all cases except for the sphere, the forces are nearly exactly proportional to the mean of the velocities squared.

The total drag coefficients were then calculated from the velocity squared line that most closely fit the data--except for the sphere. For the sphere the total drag coefficients were calculated for each individual run. The results are presented as Figure 64.

It can be seen that the drag coefficients for each case are fairly constant except at the windward 1/4 point of the wave. That is, the position 1/4 wave length upwind of the crest. At this writing it has not been determined why the total drag coefficients increase so drastically at the 1/4 wave length position upstream of the crest. The first assumption would be that the presence of the wave behind the structure did drastically change the width of the

wake. However, exhaustive vertical and horizontal traverses of the velocity profiles approaching and leaving the structures were not made. It is suggested that this be done in the future to verify the increase in total drag coefficient as noted here.

SUMMARY AND CONCLUSIONS

For determining the wind forces on the structural units of an offshore or ocean structure and for determining the total drag forces, the wind velocity profile acting on the structure should be determined. It has been shown that our knowledge of the velocity profile at sea is incomplete, to put it mildly. However, the assumption that the velocity is logarithmically distributed with elevation is commonly made and the assumption is supported by a significant amount of data.

It has been shown that total drag force coefficients and pressure coefficients are reduced when a structure is elevated on supports. The reduction in this study was 32% for the cube structure. Therefore, except for the influence of waves, the drag coefficients on elevated offshore structures should be smaller than those for ground supported structures on land. However, the testing with a solid wave built into the wind tunnel floor indicated that the drag coefficients for structures on the windward slope of a wave may be twice that for other positions on the wave. The

reason for this has not yet been determined nor is it conjectured if this will occur at sea as well as in the wind tunnel testing.

Until additional information is obtained, the recommended total drag coefficient for platform type structures with drill towers is 0.9 for nearly steady state loading with an increase to 1.4 to account for the coefficient increase on the windward face of the waves. The designer can thus possibly account for the dynamic wind loading which is caused by the undulations of the water surface below the structure. The frequency of the wind variations would be equal to the frequency of the waves. How this dynamic effect would interact with that from wind gustiness has not been determined and needs further study.

The effects from spray should be considered. For very stormy conditions the air contains a considerable amount of spray, which will add to the effective mass density and thus the momentum flux. The added force on a structure due to spray can be considerable, however, no information is available on this topic.

The drag coefficients were lower for a sphere than for other structures at all positions on the wave, which was anticipated.

The character of turbulence in the wind tunnel with the wave was not investigated. This was left for future study.

REFERENCES

1. Aiston, S. T. and J. H. Nath, "Wind Drag Coefficients for Bluff Offshore Ocean Platforms," Proceedings of the First Annual Offshore Technology Conference, Vol. I. Houston, 1969.

2. Aiston, S. T., "Wind Drag Coefficients for Bluff Offshore Ocean Platforms," M.S. Thesis, Department of Civil Engineering, Colorado State University, August, 1968.

3. Albertson, M. L., J. R. Barton, and D. B. Simons, Fluid Mechanics for Engineers, Prentice Hall, 1963.

4. Baines, W. D., "Effects of Velocity Distribution on Wind Loads and Flow Patterns on Buildings," Proceedings of Conference Held at the National Physical Laboratory, Teddington, Middlesex, June, 1963, Vol. I, Pub. by Her Majesty's Stationery Office, 1965.

5. Charnock, H., "Wind Stress on a Water Surface," Quarterly Journal of the Royal Meteorological Society, 81, pp. 639-640, 1955.

6. Cohen, E. et.al., "Wind Forces on Structures," American Society of Civil Engineers Task Committee Report, Paper No. 3269, Transactions, Vol. 126 Part II, 1961, p. 1124.

7. Davenport, A. G., "Rationale for Determining Design Wind Velocities," ASCE Transactions, Vol. 126, 1961, Part II.

8. Davenport, A. G., "Gust Loading Factors," ASCE Structural Division Journal, June, 1967.

9. Hsi, G. and J. H. Nath, "Wind Drag Within a Simulated Forest Canopy Field," Technical Report CER68-69GH-JHNG, Dept. of Civil Engineering, Colorado State University, August, 1968.

10. Kinsman, B., Wind Waves, Prentice Hall, 1965.

11. Miles, J. W., five papers on "The Generation of Surface Waves by Shear Flows," Journal Fluid Mechanics, 3 (2) 185-204, 6 (4) 568-582, 6 (4) 583-598, 7 (3) 469-478 and 13 (3) 433-448.

12. Monin, A. S., "The Atmospheric Boundary Layer," Annual Review of Fluid Mechanics, M. Van Dyke and W. G. Vincenti, eds., Vol. 2, Annual Reviews, Inc., Palo Alto, Calif., 1970.

13. Nath, J. H., and D. R. F. Harleman, "Dynamics of Fixed Towers in Deep Water Random Waves," Waterways and Harbors Division Journal, American Society of Civil Engineers, Vol. 95, WW4, November, 1969.

14. Nath, J. H., "Wind Drag Forces on Two Oceanographic Buoys," Research Report CER69-70 JHN37, Dept. of Civil Engineering, Colorado State University, June, 1970.

15. Phillips, O. M., "The Dunamics of the Upper Ocean," Cambridge University Press, 1966.

16. Roberson, J. A. and G. S. Rutherford, "Turbulence Effect on Drag of Angular Blunt Bodies," Hydraulics Division Journal of the American Society of Civil Engineers, Technical Note, Proceedings Paper 6470, March 1969

17. Roshko, A., "On the Drag and Shedding Frequency of Two-Dimensional Bluff Bodies," National Advisory Committee for Aeronautics, Technical Note 3169, Washington, D.C., July, 1954.

18. Ruggles, K. W., "Observations of the Wind Field in the First Ten Meters of the Atmosphere Above the Ocean," Report 69-1, Massachusetts Institute of Technology, Department of Meteorology, June, 1969.

19. Schlishting, H. and J. Kestin, Boundary Layer Theory, McGraw-Hill, sixth ed., 1968.

20. Seesh ltz, J. R. and E. Mollo-Christensen, "Results of a Preliminary Field Study of Wave Generation by Wind," Report 69-1 of MIT.

21. Shemdin, O. H. and E. Y. Hsu, "Dynamics of Wind in the Vicinity of Progressive Waves," Proceedings of the Tenth Conference on Coastal Engineering, Tokyo, Japan, September, 1966.

22. Sherlock, R. H., "Variation of Wind Velocity and Gusts With Height," Transactions of the American Society of Civil Engineers, 1953, pg. 463.

23. Thom, H. C. S., "Distribution of Extreme Winds in the United States," ASCE Transactions, Vol. 126, 1961, part II.

24. Wu, J., "Froude Number Scaling of Wind-Stress Coefficients," Journal of the Atmospheric Sciences, Volume 26, May, 1969.

25. Yu, Y. T., "Virtual Masses of Rectangular Plates and Parallelpipeds in Water," Journal of Applied Physics, Vol. 16, November, 1945.

TABLE 1 - DRAG COEFFICIENTS FOR CYLINDERS AND RECTANGULAR PLATES

Object	L/D	$R_e = \frac{VD}{\nu}$	C_D
Circular Cylinder, axis perpendicular to flow	1	10^5	0.63
	5		0.74
	20		0.90
	∞		1.20
	5	$>5 \times 10^5$	0.35
	∞		0.33
Rectangular	1	$>10^3$	1.16
	5		1.20
	20		1.50
	∞		1.90
Square Cylinder			
→	∞	3.5×10^4	2.0
→	∞	10^4-10^5	1.6

TABLE 2 - COMPARISON OF DRAG COEFFICIENTS FOR THE PLAIN CUBE IN THE SMOOTH WIND TUNNEL, ZERO INCIDENCE

Source	Ref. 6	Ref. 4	Shear Plate	Pressure Distribution
C_D	1.40	1.36	1.32	.24

TABLE 3 - COMPARISON OF DRAG COEFFICIENTS FOR THE ELEVATED CUBE IN THE SMOOTH WIND TUNNEL, ZERO INCIDENCE

Source	$R_e \times 10^{-5}$	C_D
Pressure Distribution	1.6	1.02
Pressure Distribution	2.6	0.96
Shear Plate	2.0	0.90
Shear Plate	2.6	0.87

TABLE 4 - COMPILATION OF AVERAGE WIND DRAG COEFFICIENTS, $\overline{C_D}$
(From Ref. 2)

δ = BOUNDARY LAYER THICKNESS h = STRUCTURE HEIGHT		δ/h	C_D		Re RANGE
			SMALL DIA. LEGS	LARGE DIA. LEGS	
PLATFORM & LEGS ONLY	LARGE MODEL	0.31	0.84	0.76	$.4 \times 10^4 - 10^6$
		1.62	0.87	0.86	$.4 \times 10^4 - 10^6$
	SMALL MODEL	1.25	0.97	0.82	$10^4 - 10^5$
		—	—	—	—
PLATFORM & LEGS W/ TOWER	LARGE MODEL	0.12	0.81	0.78	$.4 \times 10^4 - 10^6$
		0.62	0.62	0.58	$.4 \times 10^4 - 10^6$
	SMALL MODEL	0.50	0.89	0.92	$10^4 - 10^5$
		—	—	—	—
PLATFORM W/O TOWER ROUGH LEGS	K=.08"	0.31	—	0.61	$.4 \times 10^5 - .5 \times 10^6$
	=.03"	0.31	—	0.64	$.4 \times 10^5 - .5 \times 10^6$
PLATFORM W/ TOWER ROUGH LEGS	=.08"	0.12	—	0.59	$10^5 - .5 \times 10^5$
	=.03"	0.12	—	0.56	$10^5 - .5 \times 10^5$
TOWER ON PLATFORM		0	0.77	0.81	$.5 \times 10^3 - .6 \times 10^4$
		0	0.80	0.84	$.5 \times 10^3 - .6 \times 10^4$
TOWER ONLY		0.19	0.83		$.5 \times 10^3 - .6 \times 10^4$

TABLE 5 - EXAMPLE OF COMPUTED VS. EXPERIMENTAL RESULTS OF WIND DRAG FORCES ON THE COAST GUARD BUOY, METEOROLOGICAL WIND TUNNEL

Ambient Wind Velocity = 124 fps

Structural Unit	Hull	Solid Mast	Truss Work	Antenna
Projected Area (ft^2)	0.243	0.084	0.1375	0.0225
Char. Dimension (ft)	1.67	0.127	0.00693	0.0154
rms Velocity (fps)	80	110.5	124	124
Reynolds Number	6.33×10^5	6.6×10^4	4090	9100
C_D	0.35	1.2	0.94	1.12
Incr. Drag Force (lbs)	0.507	1.170	1.81	0.368

Total Computed Drag Force (lbs)	3.86
Experimentally Measured Drag Force (lbs)	3.75
% Difference	2.9%

TABLE 6 - EXAMPLE OF COMPUTED VS. EXPERIMENTAL RESULTS OF WIND DRAG FORCES ON THE OCEAN DATA STATION, METEOROLOGICAL WIND TUNNEL

Ambient Wind Velocity = 111 fps

Structural Unit	Hull	Mast	Cone Wires	Disc Rods, Etc.
Projected Area (ft^2)	0.243	0.0788	0.109	0.059
Char. Dimension (ft)	1.67	0.0433	0.00256	0.00835
rms Velocity (fps)	74.3	109.5	109.5	111.0
Reynolds Number	5.86×10^5	2.25×10^4	1330	4420
C_D	0.63	1.2	0.96	0.95
Incr. Drag Force (lbs)	0.804	1.08	1.19	0.66

Total Computed Drag Force (lbs)	3.73
Experimentally Measured Drag Force (lbs)	3.42
% Difference	9.1%

TABLE 7 - SUMMARY OF RESULTS OF COMPUTED VS. EXPERIMENTAL VALUES OF DRAG FORCES

Buoy	Tunnel	Ambient Velocity (fps)	Computed Drag Force (lbs)	Experimental Drag Force (lbs)	% Difference (%)
ODS	Met.	124	4.65	4.30	2.9
	"	111	3.73	3.42	9.1
	"	94.5	2.63	2.50	5.2
	"	78	1.89	1.75	8.0
	"	56.5	0.92	0.85	8.2
	"	49.9	0.78	0.70	11.4
	"	42.2	0.54	0.50	8.0
CGB	Met.	124	3.86	3.75	2.9
	"	111	3.53	2.82	25.0
	"	95	2.39	2.12	12.7
	"	78	1.65	1.48	11.5
	"	56.5	0.91	0.71	28.2
	"	42.0	0.51	0.43	18.6
	"	36.3	0.38	0.32	18.7
	CSU	52.9	1.06	1.05	0.9
	"	41.5	0.66	0.66	0
	"	35.1	0.48	0.47	2.1
	"	28.6	0.32	0.35	-8.6
	"	22.0	0.19	0.22	-13.6
	"	14.8	0.09	0.11	-18.2
CGB With Cone Wires	CSU	55.5	1.52	1.29	17.8
	"	52.8	1.41	1.31	8.4
	"	41.7	0.88	0.74	18.9
	"	35.6	0.64	0.50	28.0
	"	29.0	0.44	0.37	18.9
	"	22.4	0.27	0.20	35.0

TABLE 8 - RESULTS FOR THE ELEVATED CUBE ON THE FOURTH WAVE

Position	rms Velocity	C_D Legs	C_D Superstr	C_D Tower	F_D Legs	F_D Superstr	F_D Others	Pressure	Added Mass Effect	Blockage	Computed Drag	Measured Drag	Difference %
Trough	20.5	1.1	1.0		0.121	0.425		0	0	0.032	0.578	0.56	3.2
Upstream	26.7	1.2	1.0		0.225	0.725		0	0	0.055	1.005	0.95	5.8
of 4th Crest	33.65				0.356	1.160		0	0	0.080	1.60	1.52	5.3
	41.5				0.532	1.760		0	0	0.130	2.42	2.37	2.1
	53.7				0.786	2.95		0	0	0.21	3.95	3.67	7.6
¼ Wavelength	22.5				0.103	0.503		0.024	0.031	0.042	0.70	0.74	-5.4
Upstream	28.9				0.169	0.831		0.040	0.050	0.070	1.16	1.22	-4.9
of 4th Crest	36.1				0.265	1.285		0.064	0.078	0.108	1.80	1.88	-4.2
	42.2				0.361	1.770		0.091	0.104	0.140	2.47	2.53	-2.4
	55.8				0.637	3.09		0.159	0.186	0.250	4.32	4.35	-0.5
Crest	23.4				0.055	0.521		0	0	0.040	0.616	0.60	2.7
	33.9				0.114	1.085		0	0	0.085	0.285	1.23	4.5
	42.1				0.177	1.680		0	0	0.120	1.98	1.88	5.3
	50.0				0.251	2.38		0	0	0.180	2.81	2.60	8.0
	63.0				0.398	3.78		0	0	0.280	4.46	4.00	11.5
¼ Wavelength	22.3				0.095	0.50		-0.016	-0.03	0.034	0.583	0.66	-11.6
Downstream	29.4				0..65	0.88		-0.027	-0.053	0.060	1.025	1.16	-11.6
of 4th Crest	36.5				0.255	1.35		-0.042	-0.081	0.10	1.58	1.80	-12.0
	41.9				0.336	1.78		-0.055	-0.108	0.13	2.08	2.30	-9.5
	55.0	1.2	1.0		0.580	2.92		-0.098	-0.186	0.20	3.42	4.00	-14.5

selected from literature

selected from pressure distribution measurements

see ref. 24

TABLE 9 - RESULTS FOR THE SPHERE STRUCTURE ON THE FOURTH WAVE

Position	rms Velocity	C_D Legs	C_D Superstr	C_D Tower	F_D Legs	F_D Superstr	F_D Tower	Pressure Force	Added Mass Effect	Blockage	Computed Drag	Measured Drag	Difference %
Upstream Trough	21.9	1.1	0.2		0.094	0.125		0	0	0.056	0.235	0.23	2
	27.7	1.2	0.2		0.166	0.201		0	0	0.028	0.395	0.40	-1
	33.6	1.2	0.2		0.238	0.300		0	0	0.040	0.578	0.675	-14
	41.6	1.2	0.2		0.373	0.452		0	0	0.062	0.887	1.12	-21
	53.8	1.2	0.2		0.625	0.760		0	0	0.090	1.49	1.85	-19
¼ Wavelen th Upstream of 4th Crest	21.2	1.1	0.5		0.060	0.287		0.019	0.025	0.031	0.422	0.46	-8.3
	29.5	1.2	0.5		0.117	0.553		0.039	0.049	0.062	0.820	0.87	-5.75
	34.8	1.2	0.5		0.164	0.775		0.056	0.068	0.09	1.150	1.23	-6.5
	42.0	1.2	0.5		0.239	1.125		0.081	0.098	0.12	1.66	1.75	-5.1
	56.2	1.2	0.5		0.428	2.02		0.146	0.178	0.22	2.99	3.13	-4.5
Crest	25.0	1.2	0.5		0.041	0.385		0	0	0.038	0.464	0.40	16
	32.6	1.2	0.2		0.069	0.262		0	0	0.030	0.360	0.55	-35.0
	40.9	1.2	0.2		0.109	0.412		0	0	0.044	0.565	0.70	-19.0
	41.6	1.2	0.2		0.143	0.427		0	0	0.050	0.62	0.70	-11.5
	49.4	1.2	0.2		0.159	0.600		0	0	0.066	0.825	1.03	-20
	50.6	1.2	0.2		0.168	0.630		0	0	0.057	0.855	1.05	-19
	59.3	1.2	0.2		0.228	0.860		0	0	0.11	1.19	1.50	-21
	63.0	1.2	0.2		0.260	0.975		0	0	0.10	1.34	1.70	-21
¼ Wavelength Downstream of 4th Crest	23.0	1.1	0.2		0.062	0.137		-0.016	-0.031	0.012	0.164	0.15	9.3
	29.7	1.2	0.2		0.113	0.228		-0.026	-0.051	0.021	0.285	0.325	-12
	36.9	1.2	0.2		0.174	0.354		-0.040	-0.079	0.032	0.441	0.55	-20
	42.6	1.2	0.2		0.232	0.469		-0.054	-0.105	0.043	0.585	0.82	-29
	54.9	1.2	0.2		0.385	0.785		-0.089	-0.174	0.08	0.98	1.46	-33

selected from literature

selected from literature

see ref. 24

TABLE 10 - RESULTS FOR THE PLATFORM ON THE FOURTH WAVE

Position	rms Velocity	C_D Legs	C_D Superstr	C_D Tower	F_D Legs	F_D Superstr	F_D Others	Pressure Force	Added Mass Effect	Blockage	Computed Drag	Measured Drag	Difference %
Trough	22.4	1.1	0.72		0.097	0.241		0	0	0.011	0.349	0.32	9.0
Upstream	28.35	1.2			0.168	0.337		0	0	0.017	0.522	0.50	4.4
of 4th Crest	34.4	1.2			0.248	0.497		0	0 see ref. 24	0.025	0.770	0.73	5.5
	41.2	1.2			0.356	0.707		0	0	0.037	1.100	1.03	6.8
	52.5	1.2			0.555	1.180		0	0	0.055	1.790	1.61	11.2
½ Wavelength	22.5	1.2	selected from literature		0.072	0.186		0.019	0.011	0.010	0.298	0.46	-35
Upstream	29.0	1.2			0.119	0.349		0.032	0.018	0.019	0.537	0.78	-31
	35.2	1.2			0.175	0.515		0.048	0.026	0.028	0.792	1.28	-38
	41.2	1.2			0.239	0.705		0.066	0.036	0.027	1.083	1.55	-30
	54.4	1.2			0.418	1.230		0.112	0.062	0.07	1.890	2.67	-22
Crest	26.7	1.2			0.054	0.280		0	0	0.016	0.350	0.325	7.7
	33.7	1.2			0.086	0.442		0	0	0.024	0.552	0.500	10.4
	43.9	1.2			0.146	0.745		0	0	0.041	0.932	0.825	13
	50.7	1.2			0.195	1.005		0	0	0.050	1.250	1.075	21
	63.0	1.2			0.300	1.550		0	0	0.080	1.93	1.60	20
¼ Wavelength	22.2	1.1	selected from shear plate measurements with the structure on the smooth floor.		0.0615	0.211		-0.014	-0.011	0.008	0.233	0.25	-6.8
Downstream	26.6	1.2			0.096	0.298		-0.020	-0.016	0.012	0.370	0.36	2.8
	33.6	1.2			0.154	0.485		-0.032	-0.025	0.020	0.602	0.56	7.5
	40.9	1.2			0.228	0.732		-0.047	-0.037	0.030	0.906	0.85	6.6
	53.5	1.2			0.288	1.230		-0.080	-0.063	0.050	1.425	1.34	6.3

TABLE 11 - RESULTS FOR THE PLATFORM WITH TOWER ON THE FOURTH WAVE

Position	rms Velocity	C_D Legs	C_D Superstr	C_D Tower	F_D Legs	F_D Superstr	F_D Tower	Pressure Force	Added Mass Effect	Blockage	Computed Drag	Measured Drag	Difference %
Trough	21.4	1.1	0.72	0.96	0.083	0.182	0.088	0	0	0.012	0.365	0.37	-1.3
Upstream	27.0	1.2	selected from shear plate measurements with the structure on the smooth floor	0.96	0.145	0.292	0.141	0	0 see ref. 24	0.018	0.596	0.56	6.4
of 4th Crest	36.7	1.2		0.96	0.267	0.540	0.260	0		0.033	1.100	1.00	10
	41.0	1.2		0.96	0.334	0.677	0.327	0		0.047	1.385	1.27	9
	54.5	1.2		0.96	0.582	1.190	0.573	0		0.075	2.420	2.16	12
¼ Wave	21.2	1.1	selected from literature	0.96	0.056	0.175	0.056	0.016	0.009	0.011	0.323	0.47	-31
Upstream	27.2	1.2		0.96	0.099	0.289	0.093	0.027	0.014	0.020	0.542	0.76	-29
	35.2	1.2		0.96	0.168	0.487	0.156	0.045	0.024	0.033	0.933	1.25	-25
	41.9	1.2		0.96	0.236	0.552	0.222	0.065	0.034	0.040	1.15	1.75	-34
	55.1	1.2		0.96	0.407	1.190	0.382	0.093	0.058	0.080	2.21	3.00	-26
Crest	26.3	1.2	selected from literature	0.96	0.076	0.306	0.128	0	0	0.025	0.535	0.425	26
	34.3	1.2		0.96	0.124	0.495	0.207	0	0	0.039	0.865	0.725	19
	41.0	1.2		0.96	0.175	0.703	0.207	0	0	0.055	1.23	1.0	23
	47.9	1.2		0.96	0.240	0.930	0.403	0	0	0.067	1.64	1.35	21
	61.8	1.2		0.96	0.398	1.610	0.676	0	0	0.126	2.810	2.23	26
¼ Wave	21.4	1.1		0.96	0.053	0.183	0.089	-0.009	-0.009	0.010	0.317	0.3	5.7
Downstream	28.4	1.2		0.96	0.102	0.320	0.156	-0.021	-0.016	0.019	0.560	0.54	3.7
	36.2	1.2		0.96	0.161	0.527	0.254	-0.034	-0.026	0.029	0.911	0.90	1.2
	42.6	1.2		0.96	0.231	0.728	0.353	-0.047	-0.037	0.042	1.270	1.18	7.6
	54.5	1.2		0.96	0.374	1.185	0.575	-0.075	-0.060	0.070	2.07	1.87	11.0

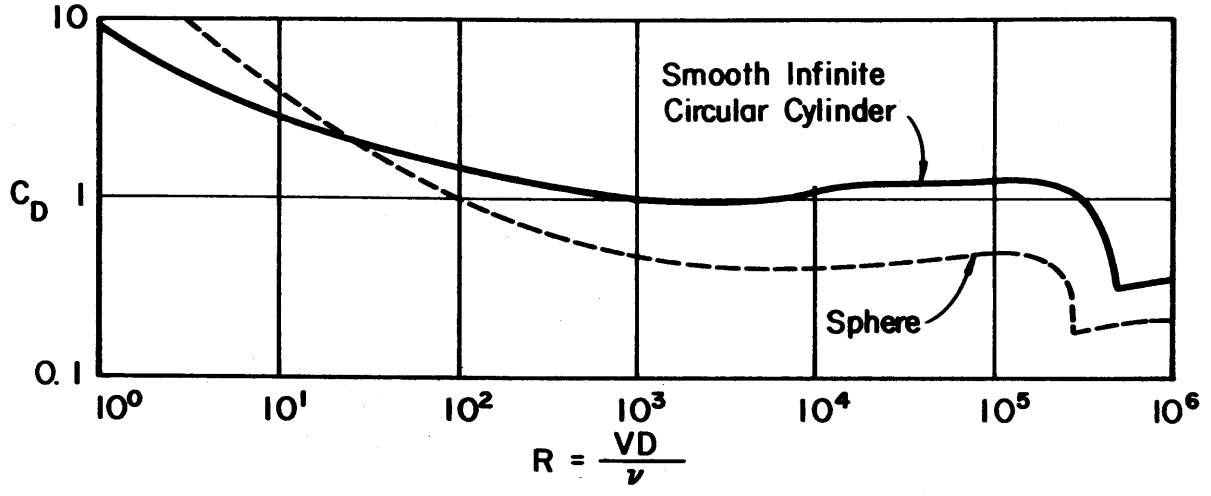

FIG. 1 - DRAG COEFFICIENT VS. REYNOLDS NUMBER FOR CIRCULAR CYLINDERS AND SPHERES.

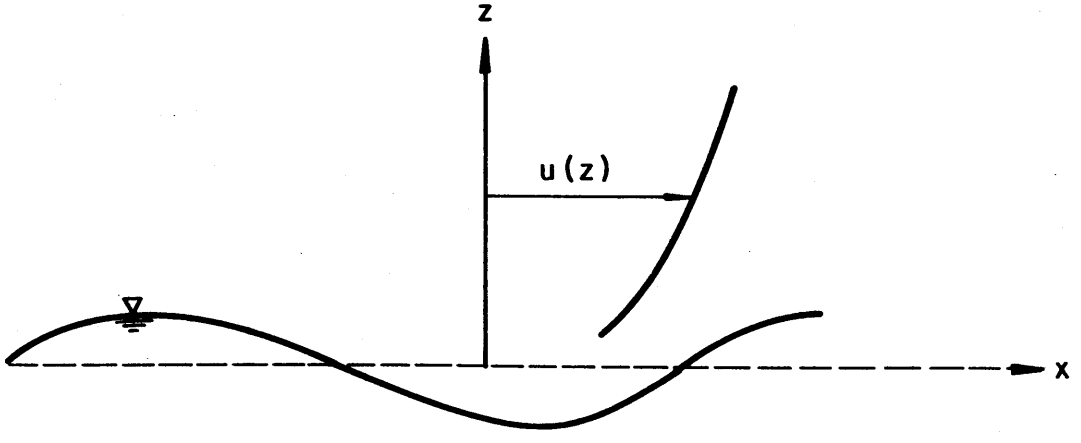

FIG. 2 - WIND PROFILE DEFINITION SKETCH

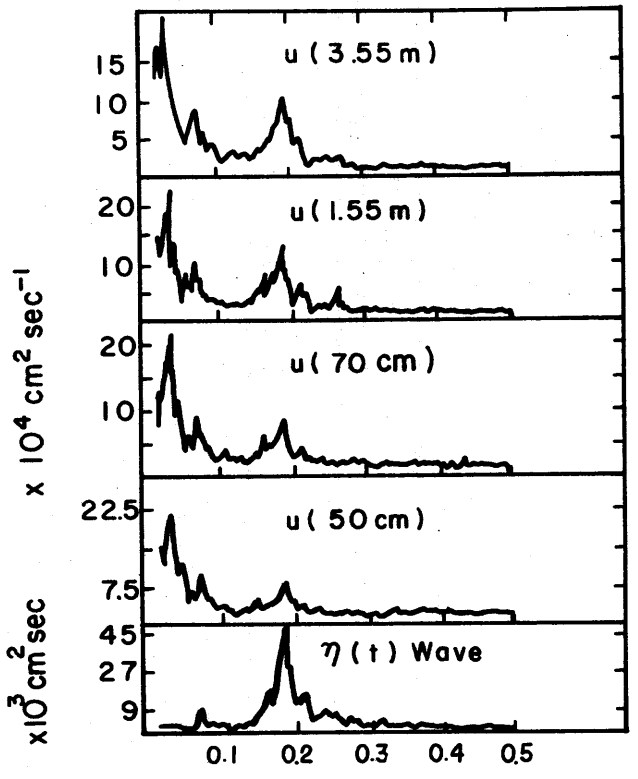

FIG. 3 - WIND SPECTRA AT DIFFERENT HEIGHTS AND CORRESPONDING WAVE SPECTRUM (From Ref. 20)

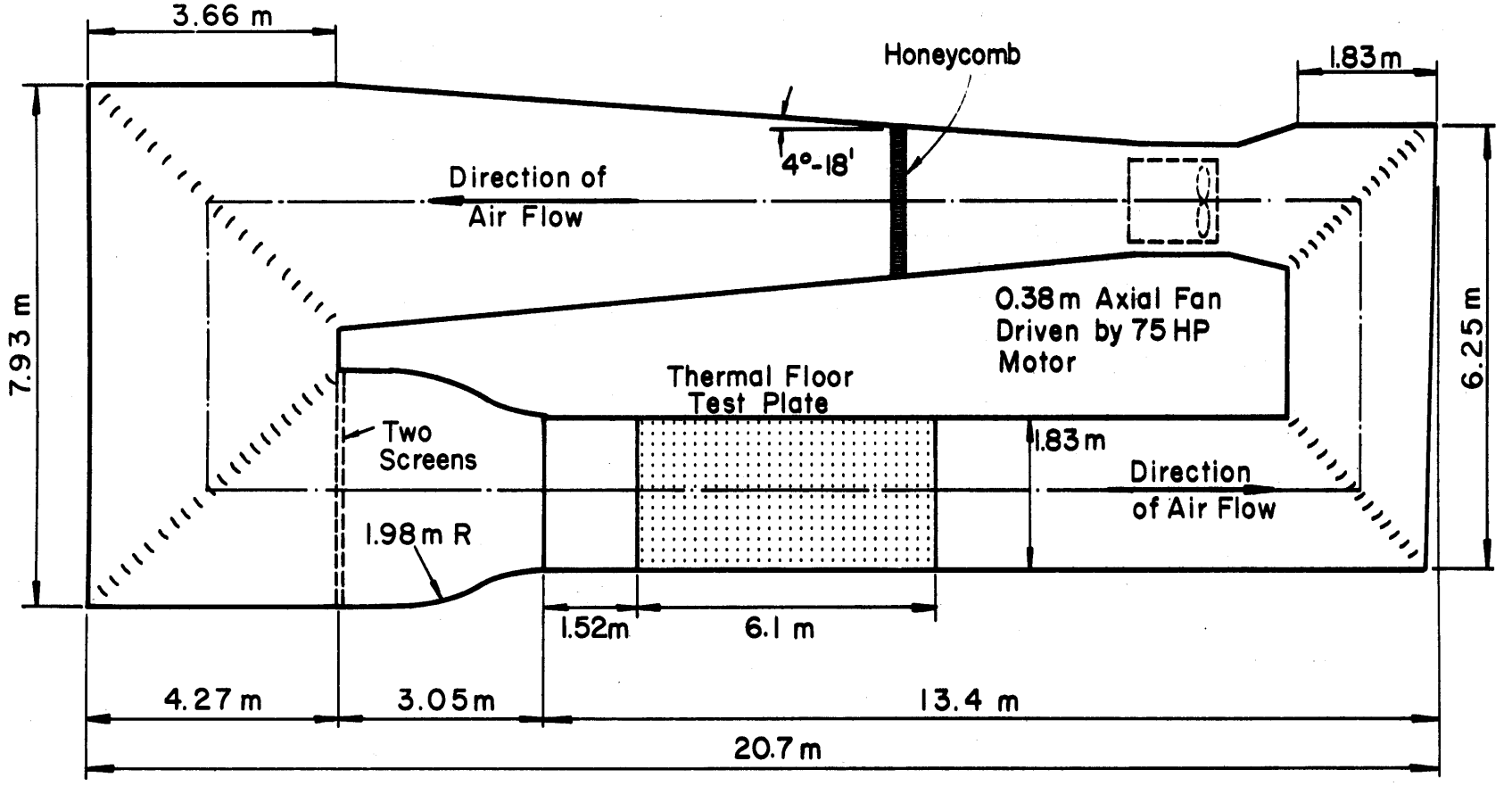

FIG. 4 - COLORADO STATE UNIVERSITY WIND TUNNEL

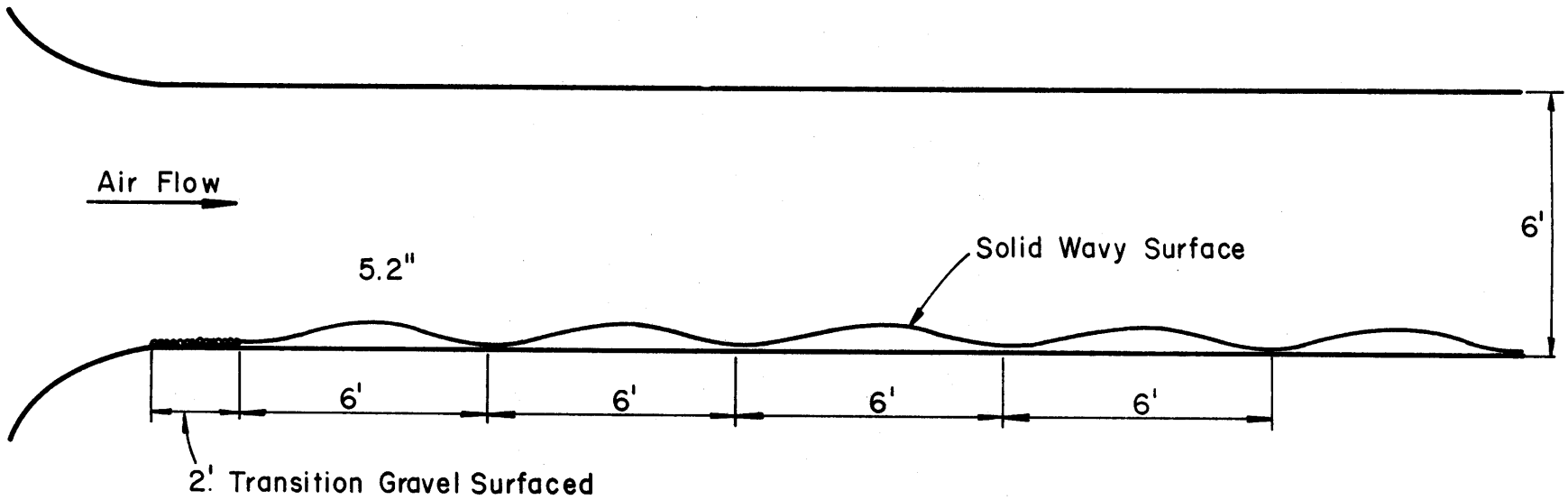

FIG. 5 - LONGITUDINAL SECTION OF THE WAVES IN THE C.S.U. WIND TUNNEL

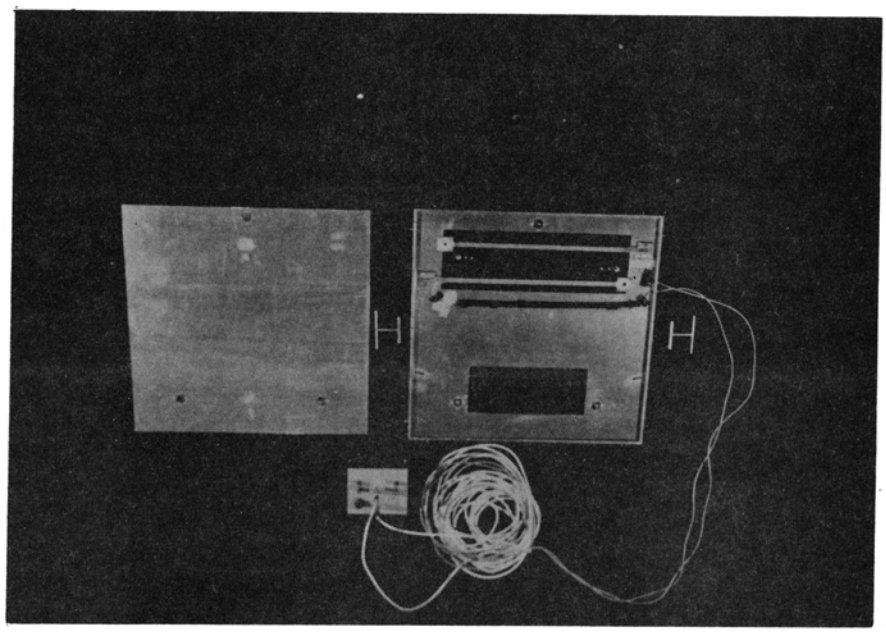

FIG. 6 - THE SHEAR PLATE

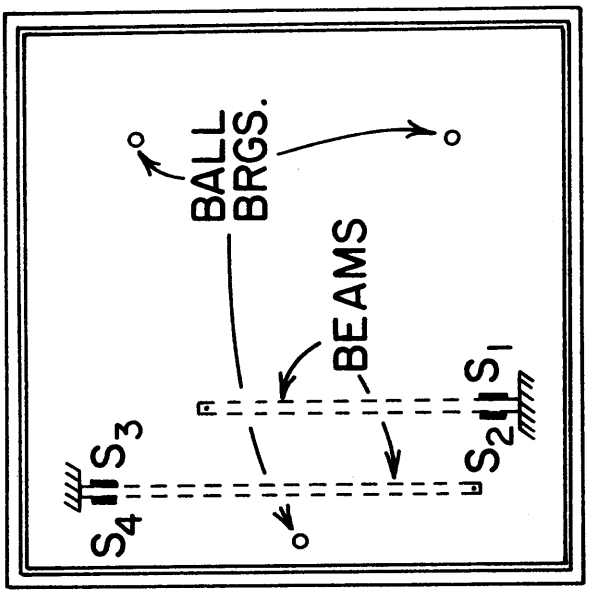

FIG. 7 - SCHEMATIC DIAGRAM OF THE SHEAR PLATE

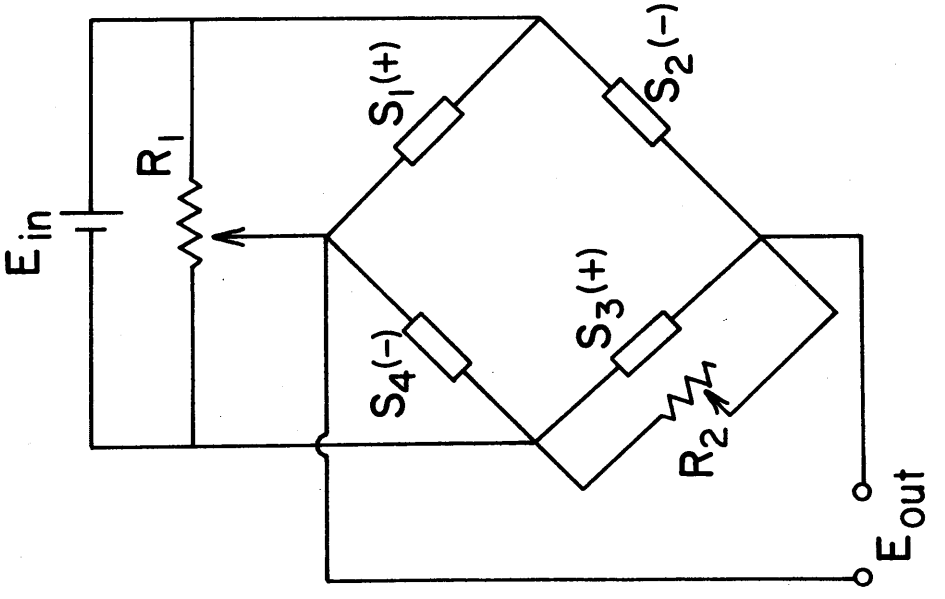

FIG. 8 - CIRCUITRY OF THE SHEAR PLATE STRAIN GAGES

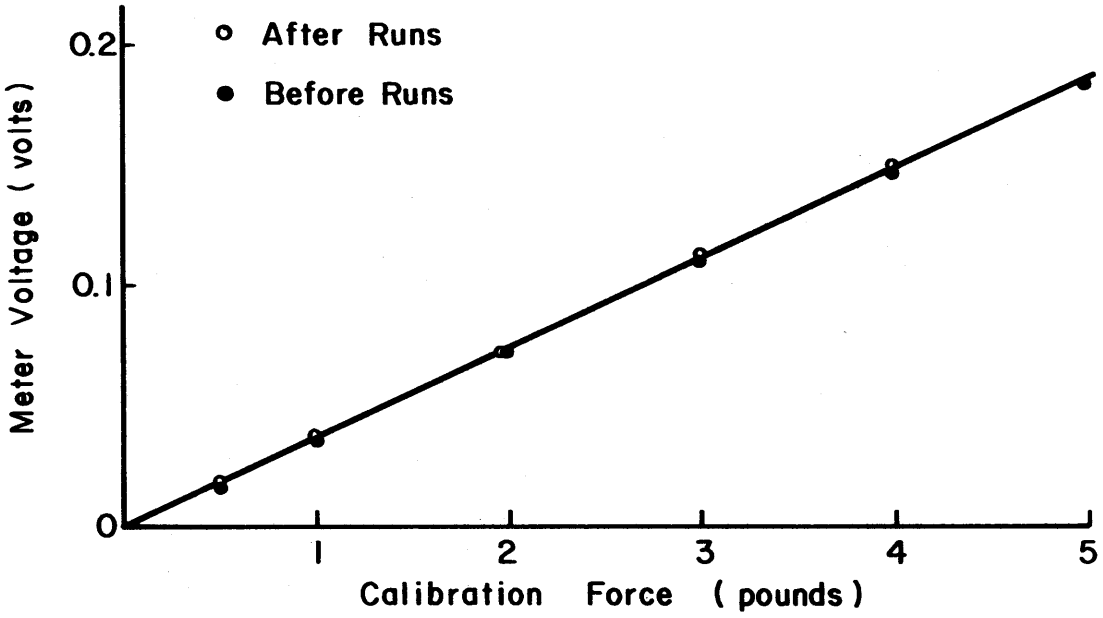

FIG. 9 - CALIBRATION-CURVE FOR THE SHEAR PLATE

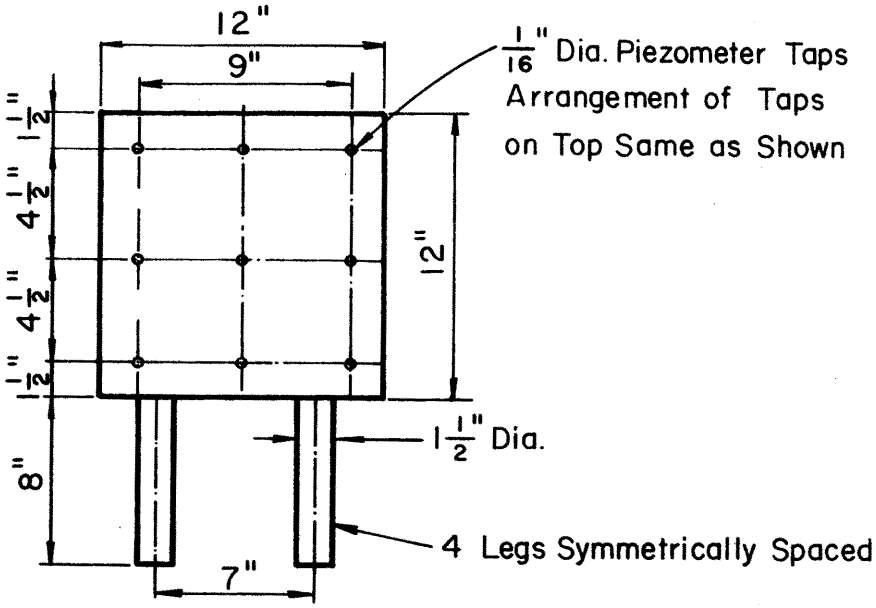

FIG. 10 - THE CUBE STRUCTURE

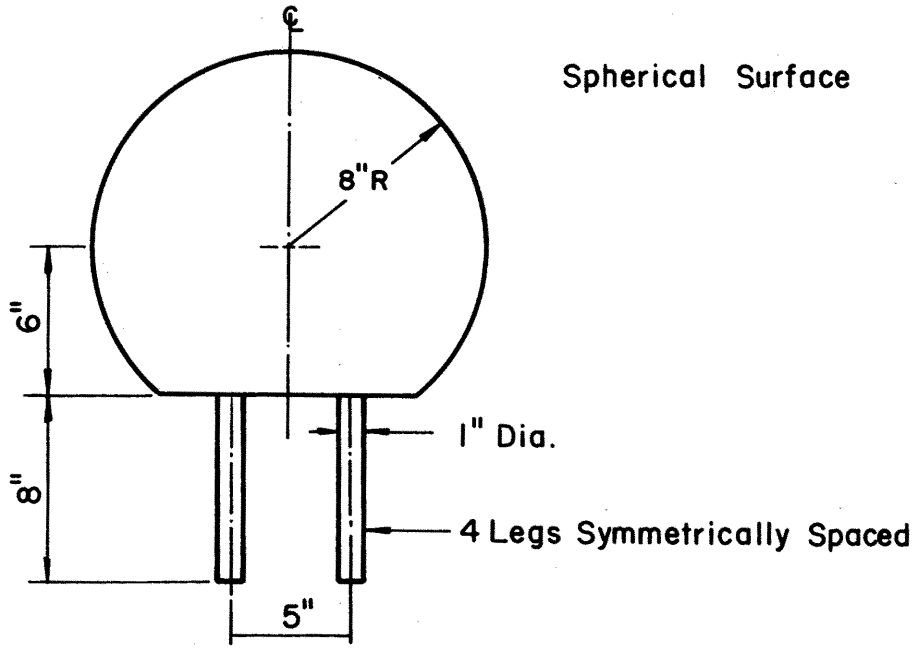

FIG. 11 - THE SPHERE STRUCTURE

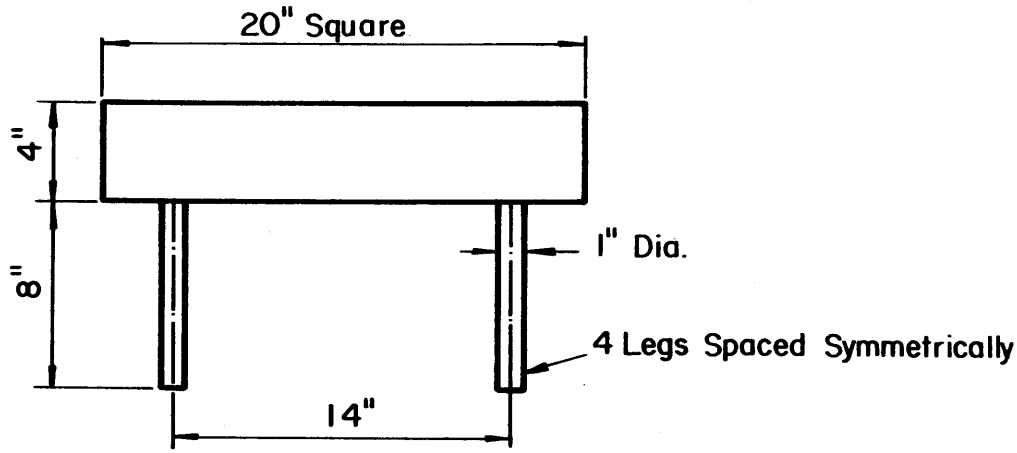

FIG. 12 - PLATFORM WITHOUT TOWER

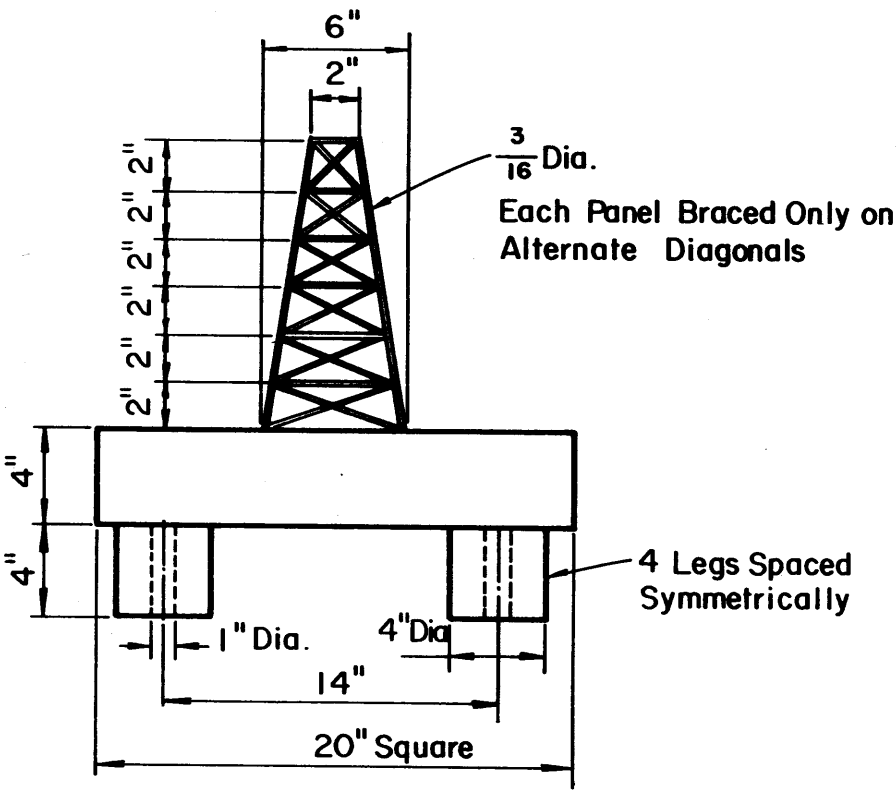

FIG. 13 - PLATFORM WITH TOWER

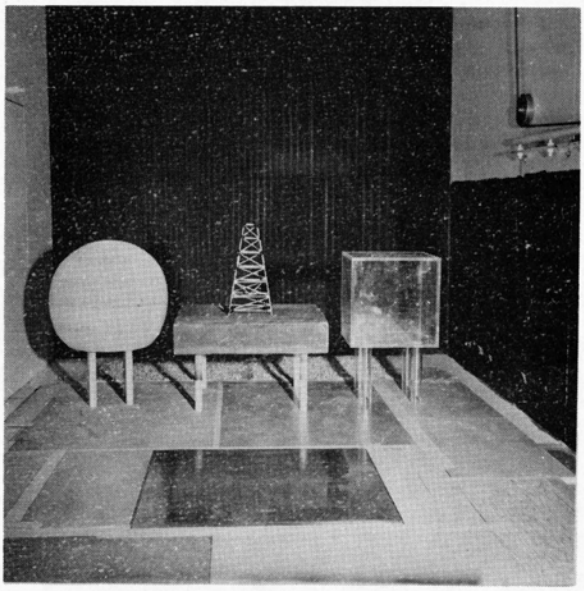

FIG. 14 - THE THREE STRUCTURAL MODELS AND THE SHEAR PLATE ON A SMOOTH FLOOR AT THE UPSTREAM END OF THE WIND TUNNEL

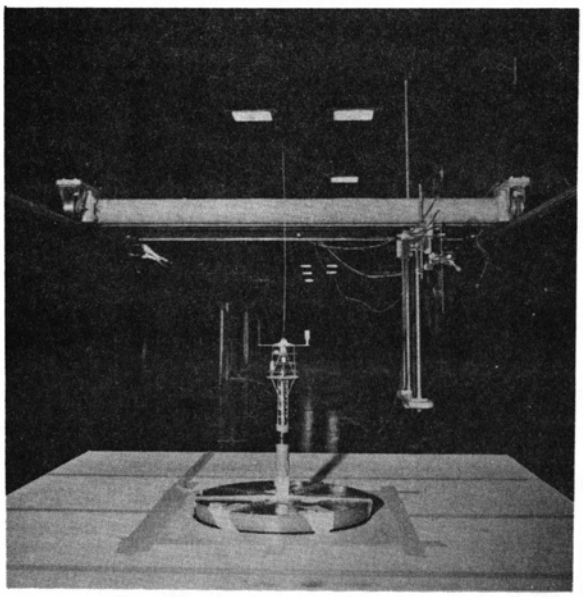

FIG. 15 - U.S. COAST GUARD BUOY MODEL IN THE METEOROLOGICAL WIND TUNNEL LOOKING DOWNSTREAM

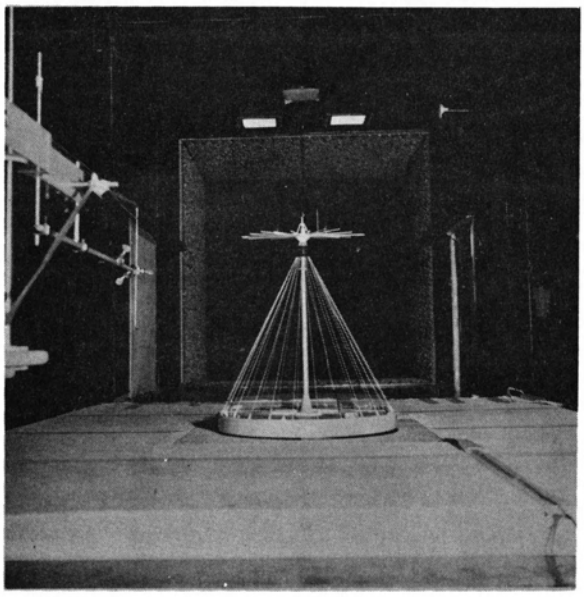

FIG. 16 - OCEAN DATA STATION BUOY MODEL IN THE METEOROLOGICAL WIND TUNNEL LOOKING UPSTREAM

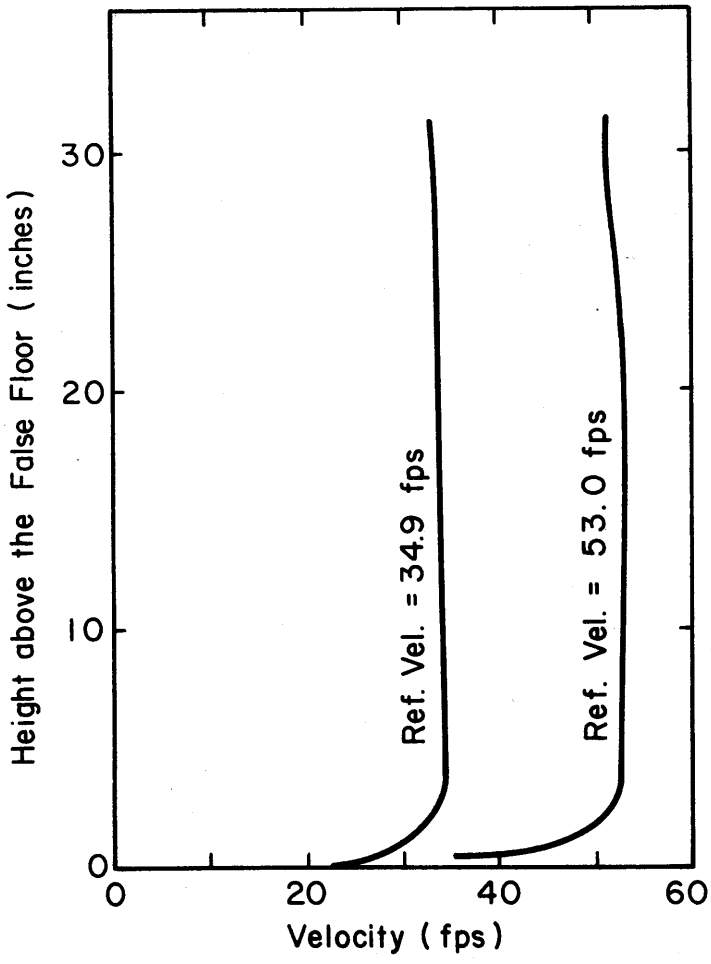

FIG. 17 - VELOCITY PROFILES IN THE C.S.U. WIND TUNNEL

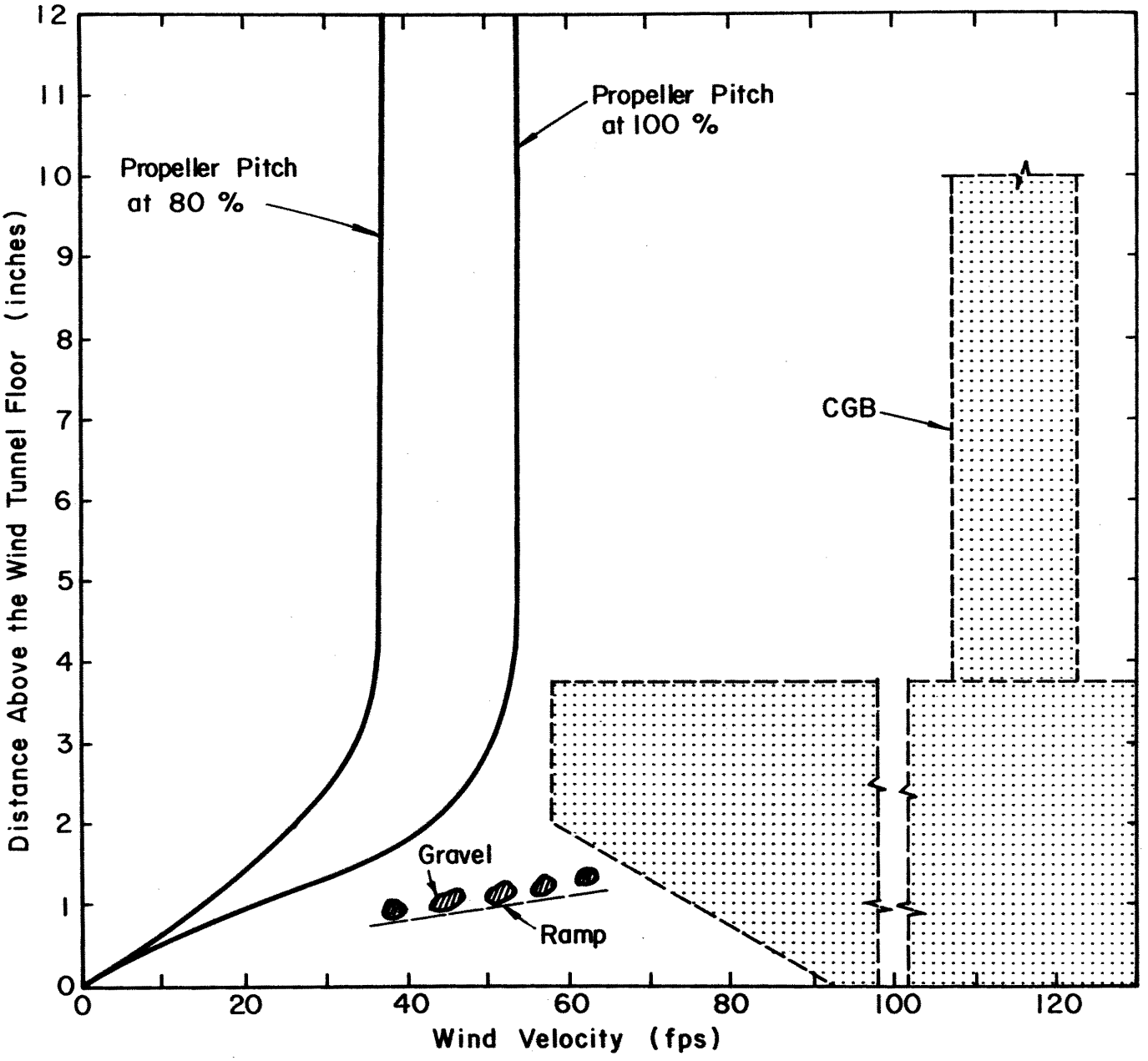

FIG. 18 - VELOCITY PROFILES AND RELATIVE POSITION OF THE CGB FOR THE C.S.U. WIND TUNNEL

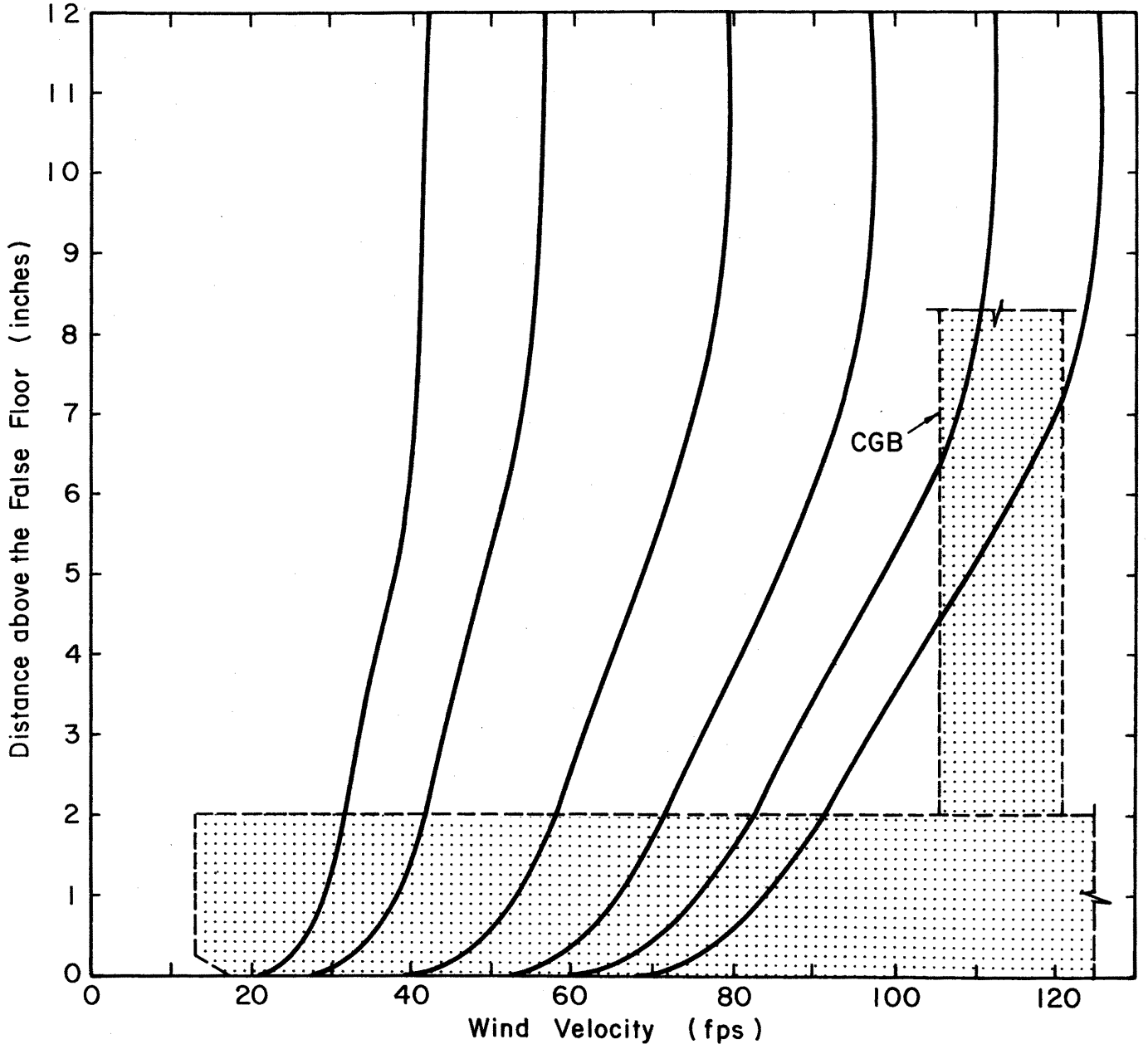

FIG. 19 - VELOCITY PROFILES AND RELATIVE POSITION OF THE CGB FOR THE METEOROLOGICAL WIND TUNNEL

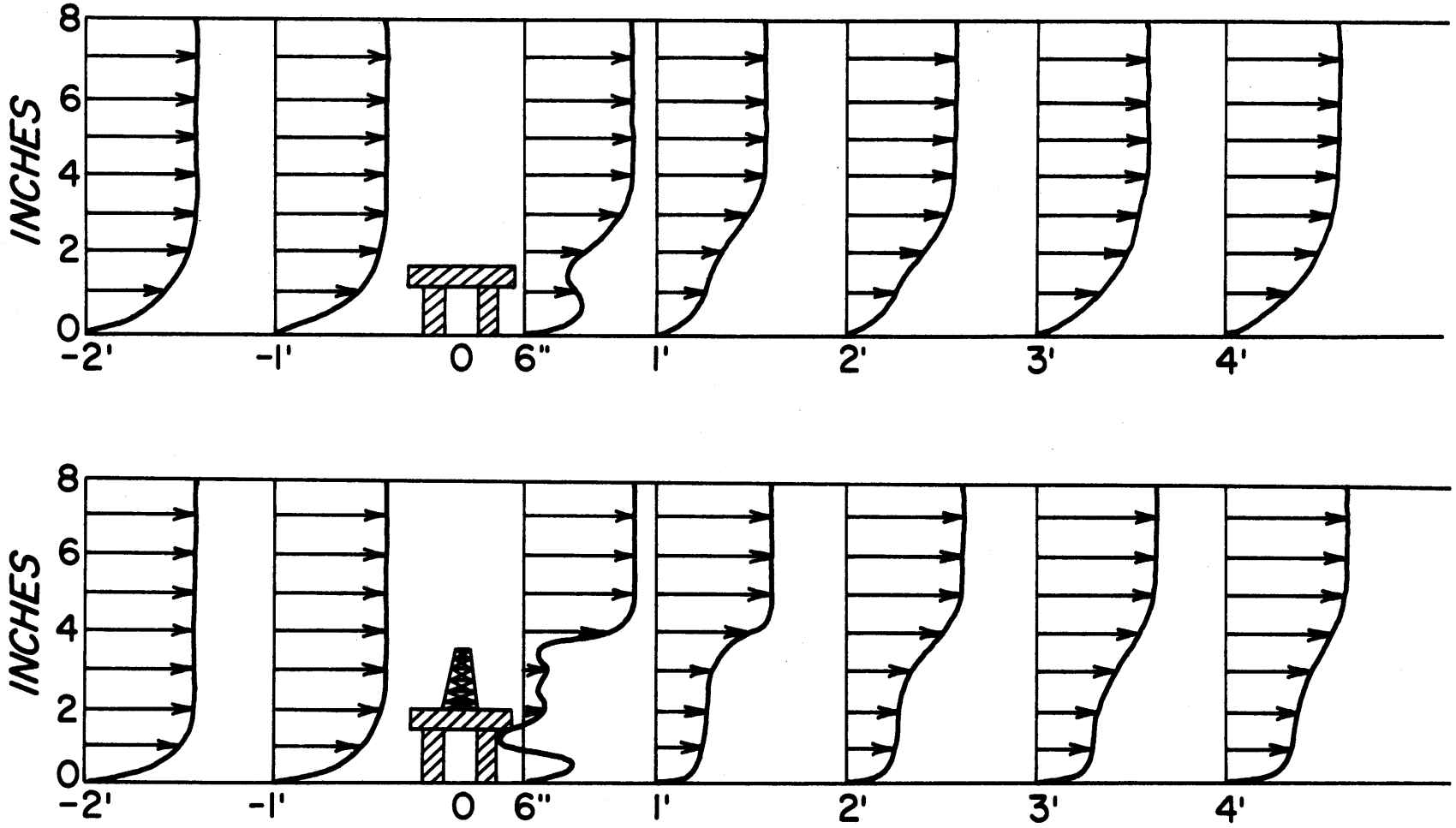

FIG. 20 - VELOCITY PROFILES UPWIND AND DOWNWIND OF A 5-INCH SQUARE PLATFORM WITH AND WITHOUT A TOWER ATTACHED

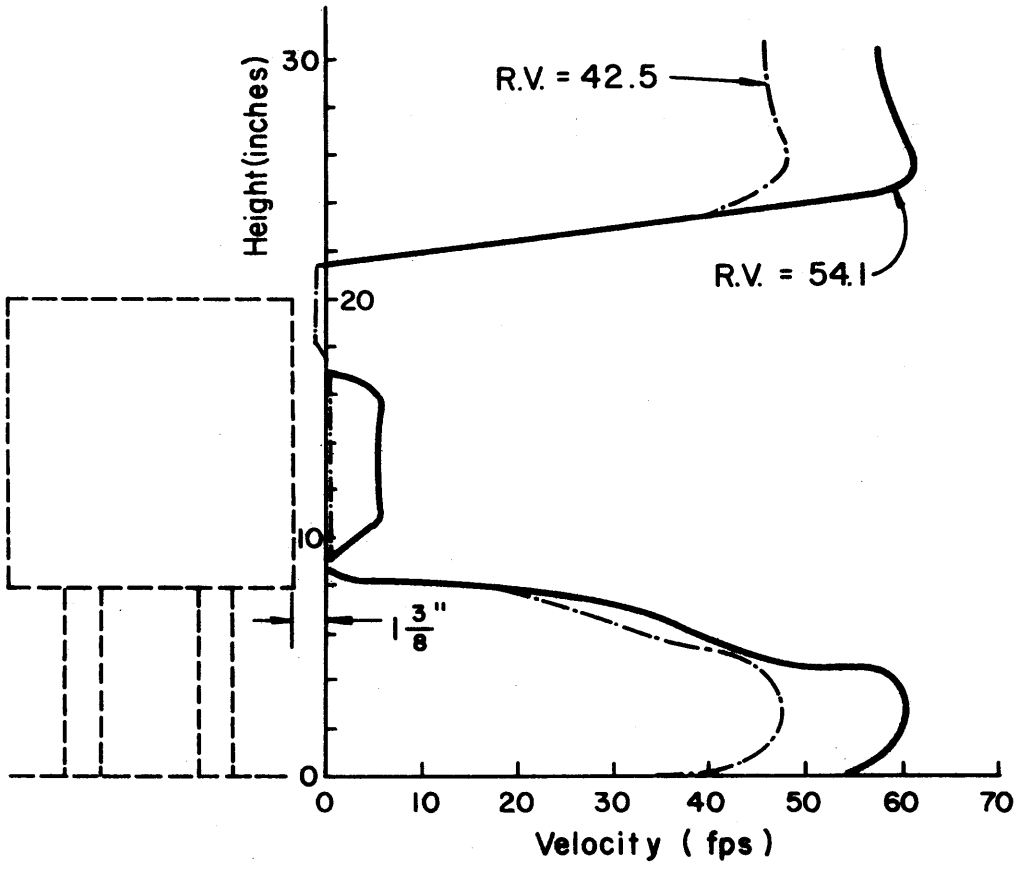

FIG. 21 - VELOCITY PROFILES BEHIND THE ELEVATED CUBE IN THE WIND TUNNEL WITH THE SMOOTH FLOOR

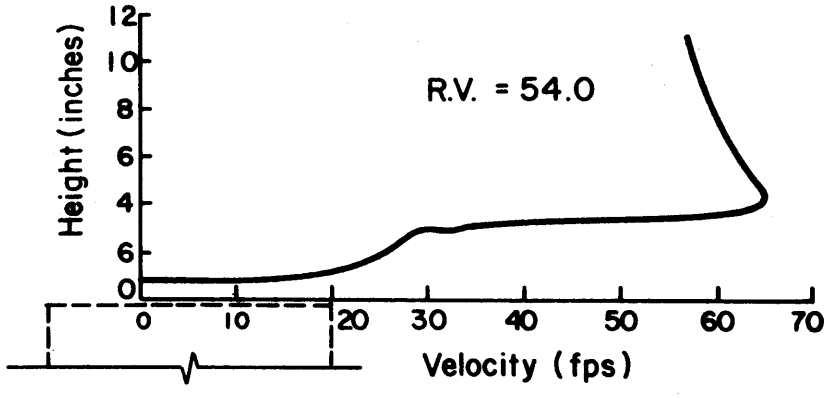

FIG. 22 - VELOCITY PROFILE TAKEN AT THE TOP OF THE ELEVATED CUBE 4" DOWNSTREAM OF THE UPSTREAM EDGE

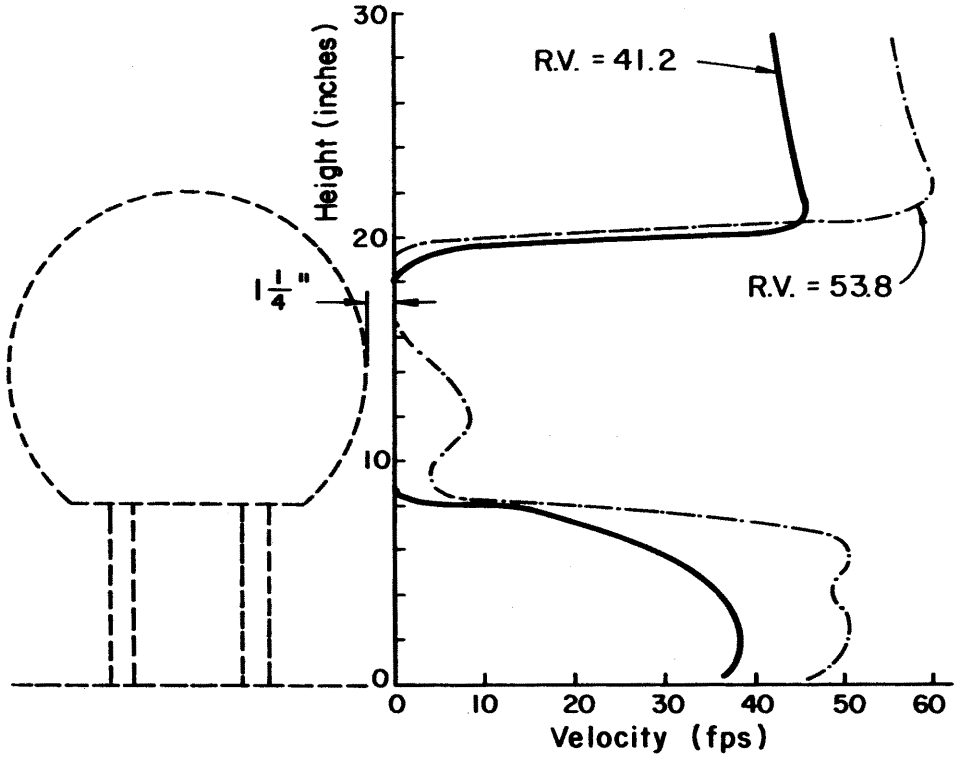

FIG. 23 - VELOCITY PROFILES BEHIND THE ELEVATED SPHERE IN THE WIND TUNNEL WITH THE SMOOTH FLOOR

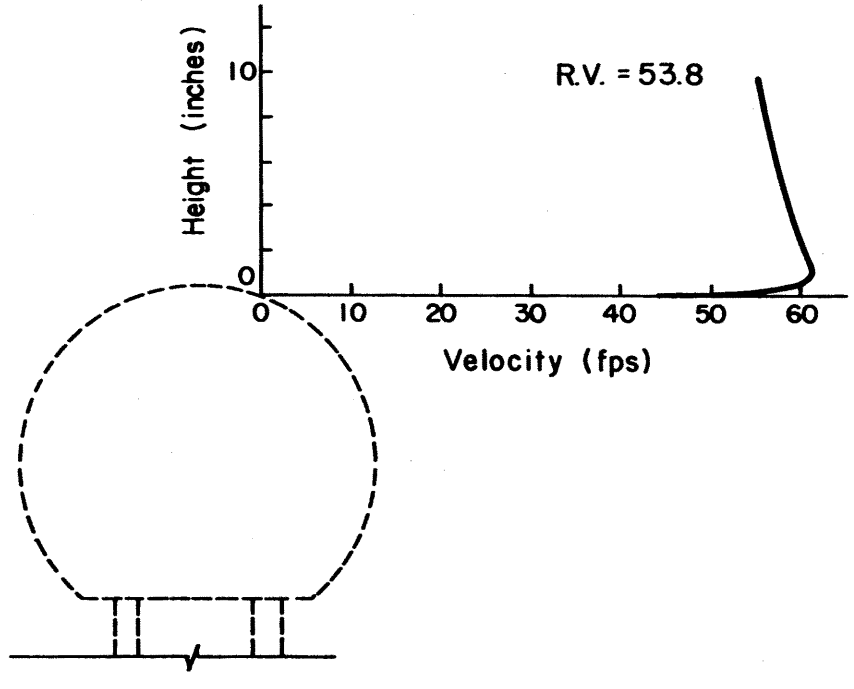

FIG. 24 - VELOCITY PROFILE TAKEN 3" DOWNSTREAM OF THE CENTER OF THE TOP OF THE SPHERE

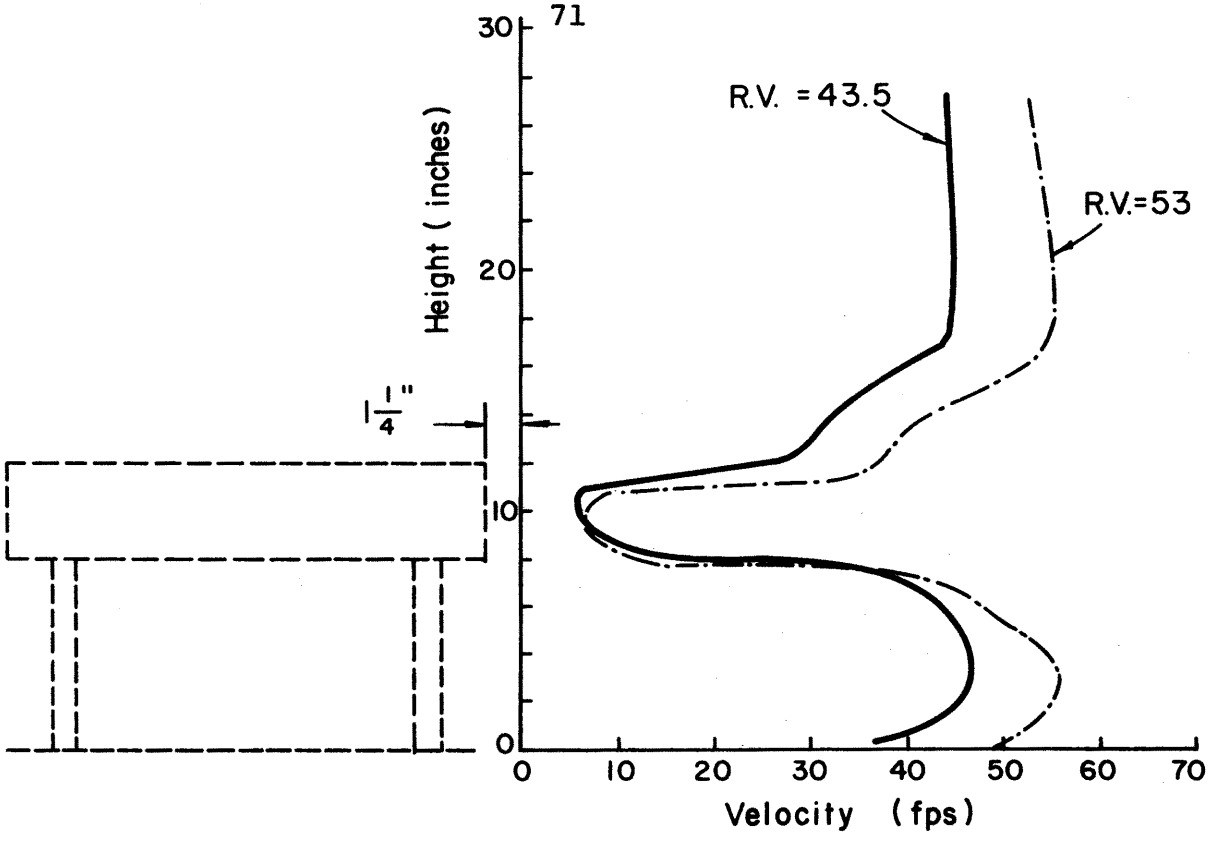

FIG. 25 - VELOCITY PROFILES BEHIND THE PLATFORM WITHOUT TOWER IN THE WIND TUNNEL WITH A SMOOTH FLOOR.

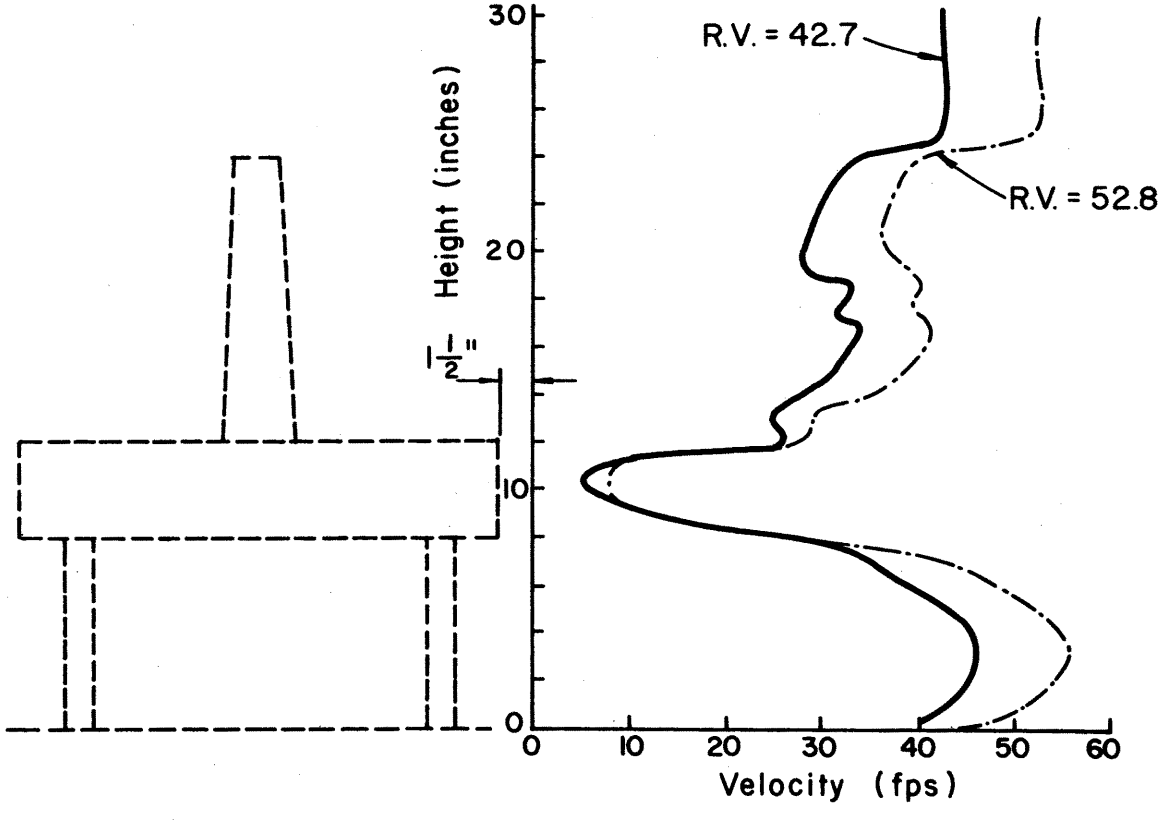

FIG. 26 - VELOCITY PROFILES BEHIND THE PLATFORM WITH TOWER IN THE WIND TUNNEL WITH A SMOOTH FLOOR